

Conserved and Divergent Features of Human and Mouse Kidney Organogenesis

Nils O. Lindström,¹ Jill A. McMahon,¹ Jinjin Guo,¹ Tracy Tran,¹ Qiuyu Guo,¹ Elisabeth Rutledge,¹ Riana K. Parvez,¹ Gohar Saribekyan,¹ Robert E. Schuler,^{2,3} Christopher Liao,¹ Albert D. Kim,¹ Ahmed Abdelhalim,¹ Seth W. Ruffins,¹ Matthew E. Thornton,⁴ Laurence Basking,⁵ Brendan Grubbs,⁴ Carl Kesselman,³ and Andrew P. McMahon¹

¹Department of Stem Cell Biology and Regenerative Medicine, Keck School of Medicine, ²Information Sciences Institute, Viterbi School of Engineering, ³Epstein Department of Industrial and Systems Engineering and Information Sciences Institute, Viterbi School of Engineering and Department of Preventive Medicine, Keck School of Medicine, and ⁴Maternal Fetal Medicine Division, University of Southern California, Los Angeles, California; and ⁵Department of Urology and Pediatrics, University of California San Francisco, San Francisco, California

ABSTRACT

Human kidney function is underpinned by approximately 1,000,000 nephrons, although the number varies substantially, and low nephron number is linked to disease. Human kidney development initiates around 4 weeks of gestation and ends around 34–37 weeks of gestation. Over this period, a reiterative inductive process establishes the nephron complement. Studies have provided insightful anatomic descriptions of human kidney development, but the limited histologic views are not readily accessible to a broad audience. In this first paper in a series providing comprehensive insight into human kidney formation, we examined human kidney development in 135 anonymously donated human kidney specimens. We documented kidney development at a macroscopic and cellular level through histologic analysis, RNA *in situ* hybridization, immunofluorescence studies, and transcriptional profiling, contrasting human development (4–23 weeks) with mouse development at selected stages (embryonic day 15.5 and postnatal day 2). The high-resolution histologic interactive atlas of human kidney organogenesis generated can be viewed at the GUDMAP database (www.gudmap.org) together with three-dimensional reconstructions of key components of the data herein. At the anatomic level, human and mouse kidney development differ in timing, scale, and global features such as lobe formation and progenitor niche organization. The data also highlight differences in molecular and cellular features, including the expression and cellular distribution of anchor gene markers used to identify key cell types in mouse kidney studies. These data will facilitate and inform *in vitro* efforts to generate human kidney structures and comparative functional analyses across mammalian species.

J Am Soc Nephrol 29: ●●–●●●, 2018. doi: <https://doi.org/10.1681/ASN.2017080887>

Studies, predominantly in the mouse and rat, have provided a mechanistic framework for mammalian kidney development; for reviews, see work by

Received August 16, 2017. Accepted November 27, 2017.

N.O.L. and J.A.M. contributed equally to this work.

Published online ahead of print. Publication date available at www.jasn.org.

Correspondence: Dr. Andrew P. McMahon, Department of Stem Cell Biology and Regenerative Medicine, Keck School of Medicine, University of Southern California, Los Angeles, CA 90089. Email: amcmahon@med.usc.edu

Copyright © 2018 by the American Society of Nephrology

Significance Statement

A poor understanding of human kidney development affects efforts to understand, model, and treat kidney disease. In this manuscript, we analyzed a large resource of human kidney samples from 4 to 23 weeks of development utilizing a variety of molecular and cellular approaches, comparing mouse and human developmental programs. A strong conservation was observed between human and mouse programs but significant differences were identified in the timing, scale, organization, and molecular profile of key cell types and composite cell structures. Together, the findings and data resource make human kidney development accessible to the biomedical community and will serve to guide translational efforts to engineer human kidney tissue.

Costantini, Kopan, Little, and McMahon.^{1–3} Genetic, molecular, and cellular analyses have provided detailed insights into the cell types, and molecular and cellular processes, engaged in kidney developmental programs. Interactions among epithelial and mesenchymal progenitor pools are responsible for generating distinct kidney components and driving kidney assembly. Progenitors within branch tips of the ureteric epithelium generate the collecting duct network for kidney drainage and the epithelial cell types within this epithelial network that regulate water, salt, and pH balance. Branching is dependent on signals from a population of metanephric mesenchyme cells capping each branch tip, whereas ureteric branch-tip–derived signals regulate the maintenance and differentiation of mesenchymal progenitor cell types. When ureteric branching commences, these mesenchymal cells comprise two lineage compartments, Six2+/Cited1+ nephron progenitors that generate all cell types of the nephron, from proximal podocytes to distal connecting segments,^{4,5} and interstitial progenitors that give rise to all interstitial cell types, mesangial cells within the glomerulus, vascular associated pericytes, and interstitial fibroblasts.^{6,7} Vascular components arise through intrinsic programs of angiogenesis initiated by vascular progenitors within the early metanephric anlagen.⁸

Kidney disease is linked to defective developmental pathways⁹ and mouse studies modeling human gene mutations with defective kidney development point to likely conservation in mechanistic aspects of mouse and human kidney development. Further evidence suggests the acquisition of CKD is linked to nephron deficiencies that mostly likely reflect underlying developmental events.¹⁰ The development-disease linkage and recent progress enabling human pluripotent stem cells (PSC) to be differentiated into a variety of kidney-like structures has rekindled interest in how the human kidney forms, the diversity of normal cell-types, and the limits to nonhuman models of kidney developmental programs.^{11–14}

Seminal histologic studies by Osathanondh and Potter,^{15–18} Oliver,¹⁹ Kampmeier,²⁰ Huber,²¹ and Peter²² underlie our current understanding of human kidney development. These studies described the emergence of key anatomic features and provided a comparative histologic view from cross-species studies of human, mouse, cat, chick, cetacean, and multiple other mammalian kidney types.^{19,22} These anatomic comparisons highlighted evolutionarily conserved features of mammalian kidney developmental programs, as well as distinct species differences. For example, variation in lobulation and the cortico-medullary architecture was suggested to reflect the evolutionary pressure for particular physiologic characteristics in mammalian species where size and the animal's environment place species-specific demands on kidney function.^{19,21,23–27}

Recognizing the importance of these early studies, there is nevertheless a need to place human kidney development in a modern molecular and cellular framework providing robust sets of data for the biomedical community. An improved understanding of human kidney development can provide

new insight into developmental and disease mechanisms, inform on conserved and nonconserved features of development from mouse to man, and provide important insight and standards for the analysis of *in vitro*–directed efforts for kidney organogenesis. For example, recent studies have documented differences in the gene regulatory programs acting within human and mouse nephron progenitors, highlighting the need for a more comprehensive view of human kidney development.²⁸

In the first of a series of papers, we assembled a developmental series of 135 kidney specimens spanning the earliest stages to midgestation, creating a publicly available histologic reference resource (www.gudmap.org). Macroanatomic and micro-niche architecture was dissected through a variety of molecular and cellular approaches. This resource will serve as a bridge to legacy data making human kidney development accessible to a modern research and clinical audience. Subsequent papers will provide an in-depth analysis of the mesenchymal progenitor populations, induction and patterning of the early nephron, and morphogenesis of the collecting duct system.

RESULTS

Our study was on the basis of 135 consented, anonymous, donated kidney specimens spanning 4–23 weeks of human kidney development. Figure 1 provides a detailed chart of the number and developmental distribution of the kidney samples and the various analyses performed at different developmental time windows.

Human renal development has previously been categorized into four phases¹⁷: phase 1 (weeks 5–15), phase 2 (weeks 14/15 to 20–22), phase 3 (weeks 20–22 to 32–36), and phase 4 (weeks 32–36 to adulthood). Over this period, the human kidney generates approximately 1,000,000 nephrons,^{10,29} although this number varies considerably, with low nephron counts likely contributing to kidney disease.^{29–33} In contrast, the mouse forms around 16,000 nephrons over a 12–13-day period of active nephrogenesis.³⁴ We focus here on the first two periods. Phase 1 begins during the embryonic developmental period, captured by the Carnegie stages (CS; approximately days 1–58, weeks 1–8).^{35–37} Within phase 1, we have focused on weeks 7–8 (CS 21–23, days 49–58), the end of the embryonic range; and in phase 2, weeks 15–17, close to the midpoint of active human nephrogenesis.³⁸ Human samples were compared with embryonic day 15.5 (E15.5) and postnatal day 2 (P2) mouse kidneys, highlighting mid and late stages of the nephrogenic program.^{34,39}

Emergence of Ureteric Branch Tips and Capping Mesenchyme

Outgrowth of the ureteric bud from the nephric duct into the adjacent metanephric mesenchyme initiates active metanephric kidney development. The interactions between epithelial tip

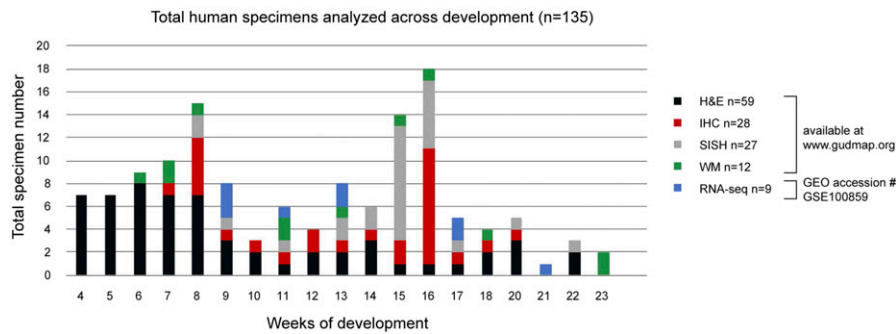


Figure 1. Summary of samples used in the study. Graphed data for specimens used for H&E, SISH, IHC, whole-mount (WM), and RNA-seq. H&E, Hematoxylin and eosin; IHC, Immunohistochemistry; SISH, Section in situ hybridization; RNA-seq, RNA-sequencing.

and kidney progenitor types within the metanephric mesenchyme drive assembly of the mammalian kidney.^{1–3,40} Our focus herein lies in providing an overview of human kidney organogenesis: organizational changes within the branching collecting duct network, capping mesenchymal populations, and nephrogenic program. Detailed molecular and cellular analyses of each of these events will be discussed separately.

In the mouse, outgrowth of the ureteric bud into an adjacent prespecified population of metanephric mesenchymal progenitors, the initiating event in kidney morphogenesis, commences at E11 (Supplemental Figure 1A). Potter²³ reported human metanephric kidney development beginning at CS13, approximately 4 weeks postfertilization (embryo crown-to-rump length of 5 mm). Consistent with this view, a single nondivided, bulbous-shaped ureteric bud outgrowth surrounded by metanephric mesenchyme was observed in the CS13 embryo (Figures 2A). By CS16, the bud generated one to two branches with cap mesenchyme cells tightly clustered around each branch tip (Figures 2B and 5A), resembling the E12.5 mouse kidney (Supplemental Figure 1B). In contrast to the mouse, the branching human ureteric epithelium was bilayered from CS13 to CS16 (Figures 2, A and B, and 5A). By CS19, ureteric branch tips were unilaminar and physically distinct mesenchymal cell populations that likely harbor the nephron progenitors, cap each branch tip (Figures 2C and 5B), a persistent arrangement maintained to 23 weeks, the latest stage studied (Figures 2, 3, 5 and 7). During the CS16–CS22 period, branch tips adopt a “T” or “Y” shape (Figure 2, B–D). The ureteric branch tip morphology changed at around CS23 when tips showed a pronounced expanded morphology with a prominent lumen (Figures 2E, 4, A and F, and 5D). This tip reorganization persisted to week 9 (not shown) but was not observed beyond week 10 (Figure 3, A and B). After CS23, tips maintained a “V”-shaped morphology to week 16 (Figure 3, A–D).

The Human Nephrogenic Niche Is Distributed across Lobular and Interlobular Regions of the Kidney Cortex
Unlike the mouse, the human kidney is comprised of multiple lobes.^{19,23} The region between lobes has previously been

suggested to form the “column of Bertin,” but Potter argues that a better term might be “sheets of Bertin” because they are the surfaces of two nephrogenic zones.²³ Because these regions are simply the meeting point of two peripheral curvatures of kidney cortex, we refer to these as interlobular folds or interlobular regions. Lobulation is first detected at CS19 with the appearance of striations between anterior and posterior kidney domains (Figure 2C). The stromal striations described here contrast with the view of Potter.²³ The cortical surfaces of the kidney indent from CS20–CS23 (Figure 2, D and E), and visible lobes become morphologically pronounced as additional lobe folds appear from 10 to 16 weeks (Figure 3).

To further examine the nephrogenic niches at peripheral and interlobular regions, we performed an immunofluorescent analysis to detect cell types characteristic of the mouse nephrogenic niche. The earliest samples compatible with immunodetection were CS23 kidneys. At this time, a dense population of SIX2+ nephron progenitor cells surrounded the ureteric epithelial tips (Figure 4A), similar to the organization documented in the week 16 human kidney.²⁸ This progenitor population was 2–7 cell-layers thick (arrowheads in Figure 4A), the thicker portions located to the sides of the ureteric epithelial branch tips. The cells closest to the tip were polarized, with their long axis approximately perpendicular to the tip, whereas other SIX2+ putative progenitors were rounded without an elongated nucleus. At 15 weeks, 2–3 layers of SIX2+ nephron progenitors were tightly packed around each ureteric epithelial tip (Figure 4, B and C, Supplemental Figure 2A). SIX2+ cells show a specific organization, with long axes of cells closest to the ureteric epithelial tip orientated at right angles to branch tips (Figure 4, B and C). Peripheral and interlobular regions displayed a similar morphology (Figure 4, B and C).

The architecture of the E15.5 mouse nephrogenic niche resembled that of CS23 and week 15 human kidneys, although smaller in size with fewer SIX2+ cells (Figure 4D). The P2 mouse nephrogenic niche was distinctly different from human stages examined here; the few SIX2+ cells around the tips morphologically resembled pretubular aggregates (PTAs) and renal vesicles (RVs), early committed stages in the nephrogenic program (Figure 4E; see later discussion of human

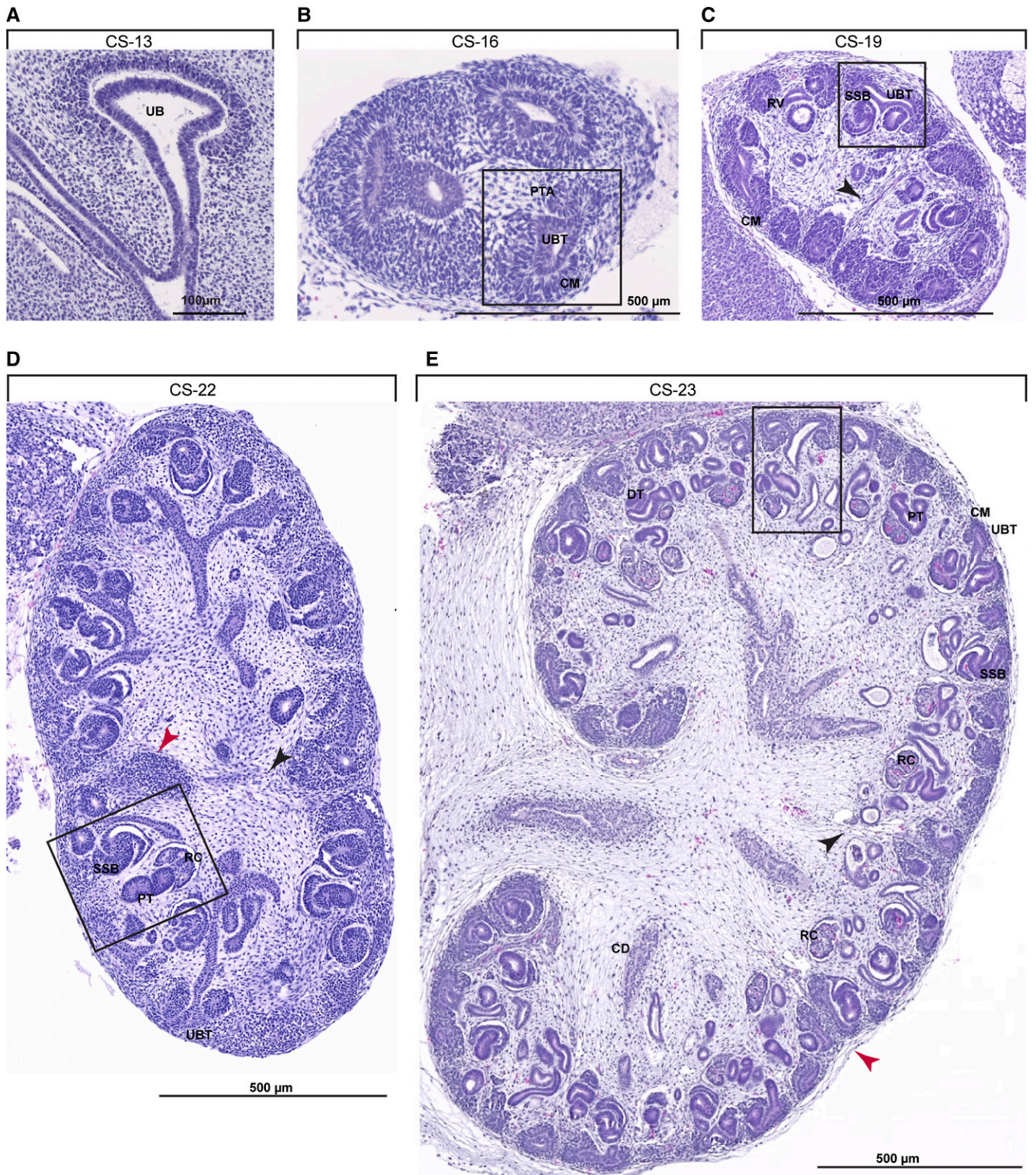


Figure 2. Histologic analyses of human kidney development show emerging complexity in the human kidney. (A–E) Hematoxylin and eosin staining of human kidneys from CS13 to CS23. Scale bars as indicated on fields. Black arrowheads point to cell striations, red arrowheads point to surface indentations. Boxed areas shown in Figure 5. CD, collecting duct; CM, cap mesenchyme; DT, distal tubule; RC, renal corpuscle; UB, Ureteric bud epithelium; UBT, ureteric bud tip.

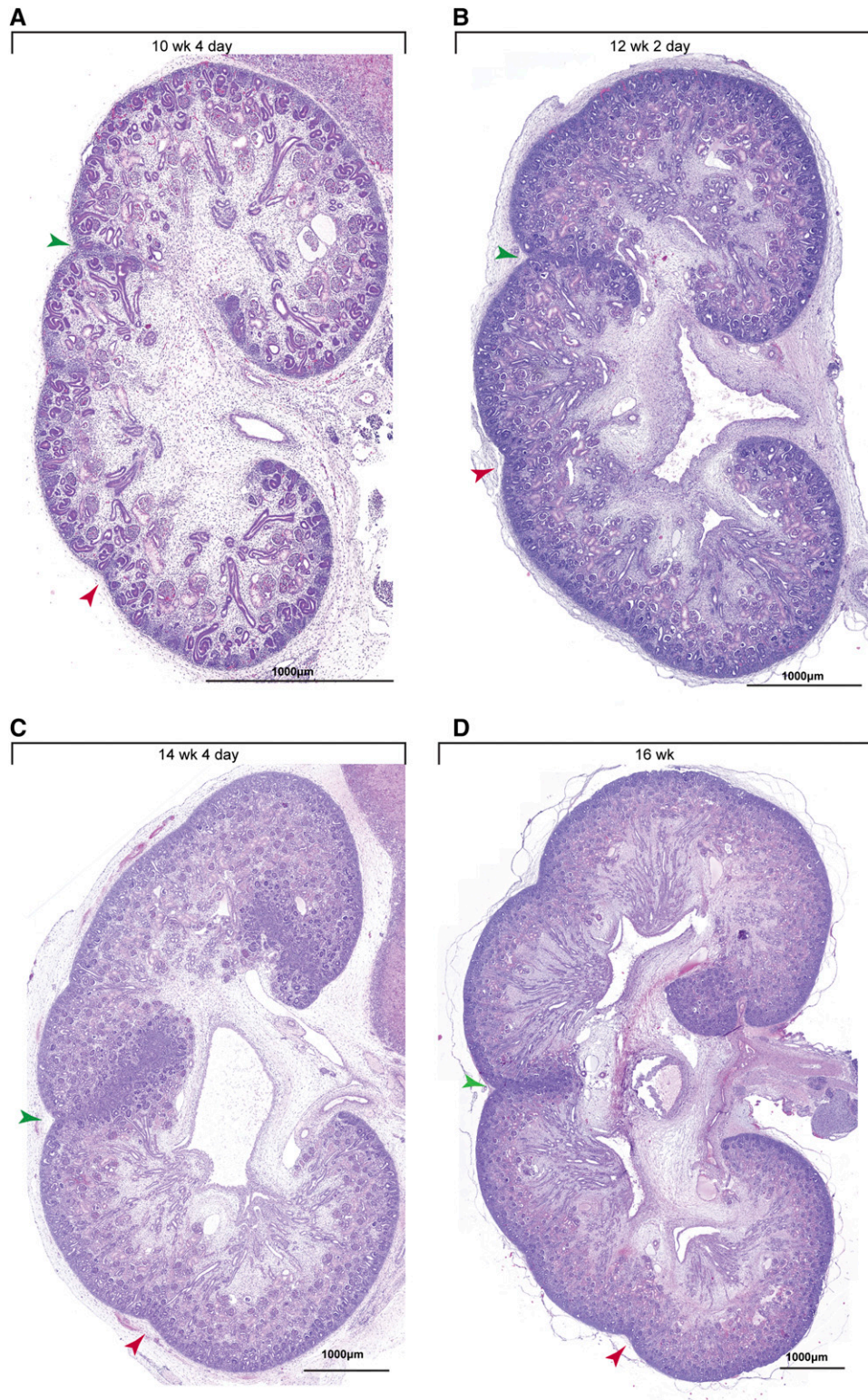


Figure 3. Histologic analyses of human kidney development show emerging complexity in the human kidney. (A–D) Hematoxylin and eosin staining of human kidneys from week 10 to week 16. Scale bars as indicated on fields. Red arrowheads point to surface indentations, green arrowheads point to lobe folds.

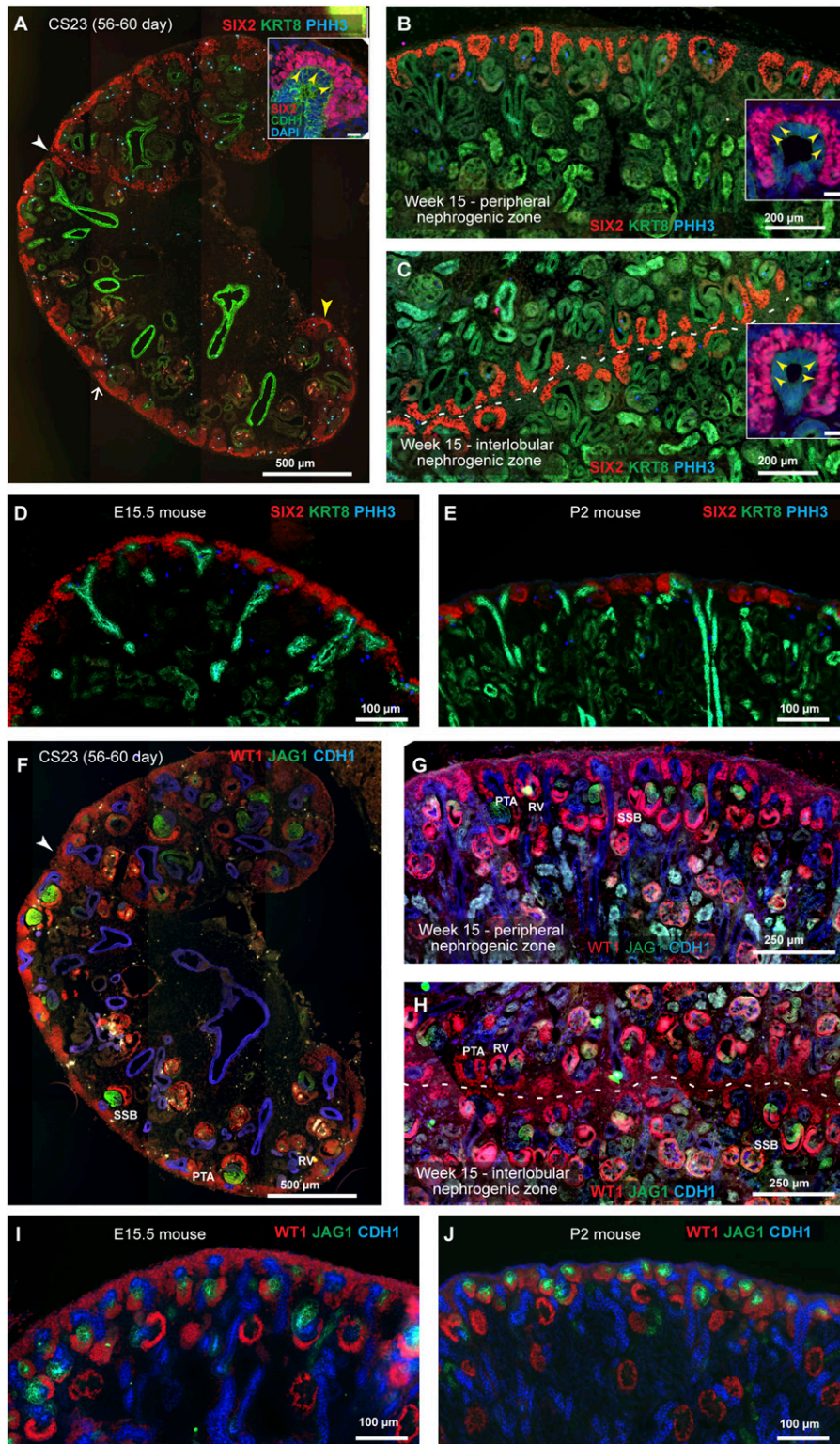


Figure 4. Immunofluorescent characterization of early human kidney development and lobulation show conserved and divergent features. (A–C) Sagittal sections of a week 8 (CS23) and week 15 kidney with immunofluorescent labeling for SIX2, KRT8/18, and PHH3 (insert shows high magnification of week 8 tip and nephron progenitors; scale bar, 20 μ m). (B and C) Peripheral and interlobular regions of week 15 cortex, respectively. Inserts show high magnification of tips with surrounding nephron progenitors. Scale bars in inserts are 20 μ m and inserts show SIX2, KRT8, and DAPI stain. Arrowheads in inserts point to polarized progenitor cells. Equivalent stains for mouse E15.5 and P2 are shown in (D and E). (F–H) Sagittal section of a week 8 (CS23) and week 15 kidney with staining for WT1, JAG1, CDH1, and DAPI. Labels PTA, RV, and SSB indicate proximal tubule, renal vesicle, and subcapsular boundary, respectively. Scale bars are 500 μ m (F), 250 μ m (G, H), and 100 μ m (I, J).

Table 1.

Ontology of early human renal development during Carnegie Stages for analysis of early development

| Carnegie Stage | CS13 | CS15 | CS16 | CS18 | CS18-19 | CS19 | CS21 | CS22 | CS23 |
|--|-------|-------|--------|---------|---------|---------|---------|---------|---------|
| Crown rump length | 4-6mm | 7-9mm | 8-11mm | 13-17mm | 13-18mm | 16-18mm | 22-24mm | 23-28mm | 27-31mm |
| Days post ovulation | 28-32 | 33-37 | 37-41 | 44-47 | 44-51 | 48-51 | 52-54 | 54-56 | 56-60 |
| Ontology | | | | | | | | | |
| mesonephros (EHAPA:16744) | | | | | | | | | |
| metanephric mesenchyme (EHAPA:17375) | | | | | | | | | |
| ureteric bud (EHAPA:17209) | | | | | | | | | |
| cap mesenchyme (EHAPA:27621) | | | | | | | | | |
| ureteric tip (EHAPA:27605) | | | | | | | | | |
| ureteric stalk (EHAPA:27608) | | | | | | | | | |
| pretubular aggregate (EHAPA:27673) | | | | | | | | | |
| renal vesicle (EHAPA:27678) | | | | | | | | | |
| comma-shaped body (EHAPA:27681) | | | | | | | | | |
| s-shaped body (EHAPA:27756) | | | | | | | | | |
| capillary loop renal corpuscle (EHAPA:27770) | | | | | | | | | |
| early proximal tubule (EHAPA:27784) | | | | | | | | | |
| early distal tubule (EHAPA:27788) | | | | | | | | | |
| mature renal corpuscle (EHAPA:28236) | | | | | | | | | |
| collecting duct (EHAPA:28407) | | | | | | | | | |
| renal capsule (EHAPA:18679) | | | | | | | | | |
| Interstitium striations | | | | | | | | | |
| Surface indentations | | | | | | | | | |
| Lobe folds | | | | | | | | | |
| Number of Specimens | 1 | 3 | 1 | 4 | 1 | 3 | 4 | 2 | 7 |

EHAPA, Edinburgh Human Anatomy Project Atlas.

nephrogenesis). In the mouse, MEIS1+/FOXD1+ cells demarcate the interstitial progenitor pool that lies above the SIX2+ nephron progenitors beneath the kidney capsule (Supplemental Figure 2C^{7,41}). A similarly positioned SIX2−; MEIS1+ population of putative interstitial progenitors was observed in the human kidney, with SIX2−; MEIS1+ cells separating adjacent SIX2+ nephron progenitor niches in interlobular regions (Supplemental Figure 2, D and E).

To broadly examine active nephrogenesis we visualized JAG1, a marker for nascent nephrons,⁴² and WT1, a marker of interstitial and nephron progenitor cell types that in the mouse shows polarized activity in early RVs prefiguring a role in podocyte development (Figure 4, I and J). We observed a continuous active program of nephrogenesis across interlobular (15 weeks) and peripheral regions (CS23 and 15 weeks) of human kidneys (Figure 4, F–H, Supplemental Figure 2B). In conclusion, the similarities in cell morphology, cell types, and cell organization suggest peripheral and interlobular mesenchymal niches follow similar programs in the human kidney. Further, clear parallels are evident in the organization of nephrogenic niches between mouse and man.

The Formation of the First Generation of Nephrons and Organization of the Ureteric Epithelial Network

To characterize the process of nephrogenesis in broad detail, we first examined histologic preparations for structural features indicative of the nephrogenic program. In the mouse, the first physical evidence of nephron commitment is the appearance of a tightly clustered group of cells, the PTA, beneath

the ureteric branch tip.⁴³ Thereafter, the PTA forms an epithelial nephron precursor, the RV, which transitions through a complex morphogenesis to an S-shaped body (SSB) nephron anlagen with a patent luminal connection to the adjacent collecting duct network.³

The emergence of different structures and anatomic features during the first nephrogenic events are summarized in Table 1. Evidence of human nephrogenesis was first observed at CS16 (Figure 5A), with PTAs beneath the ureteric branch tips resembling those of the E12.0 mouse kidney (data not shown). By CS19, PTAs, comma-shaped bodies, and SSBs were observed beneath the ureteric branch tips (Figure 5B). The connection of the nephron to the ureteric epithelium was evident by the SSB stage. At CS19 it was possible to find a maximum of two generations of developing nephrons per tip; *e.g.*, a PTA and an SSB. Capillary loop–stage nephrons were first detected at CS22, by which time three generations of nephrons were observed; *e.g.*, a PTA, an SSB, and a capillary loop nephron (Figure 5C). Capillary loop–stage nephrons at CS23 were extensively vascularized, indicative of a mature glomerular organization, but showed a rudimentary associated tubular network (Figure 5D). Subsequent developmental time-points exhibited further nephron generations and maturation of the renal corpuscles (Figure 5, E–H).

On the basis of the first appearance of a structure, progression from the first PTA to a connected SSB takes between 3 and 14 days: the shortest and longest time intervals between CS16 and CS18 stages, and a further 1–10 days to a capillary loop–stage

and CDH1. (G and H) Peripheral and interlobular regions of week 15 kidney cortex, respectively. (I and J) Equivalent stains for mouse E15.5 and P2 stages. White arrowheads point to lobe folds, open arrows point to multilayered cap mesenchyme, and yellow arrowheads point to polarized progenitors around tips. White dashed lines demarc where lobes meet.

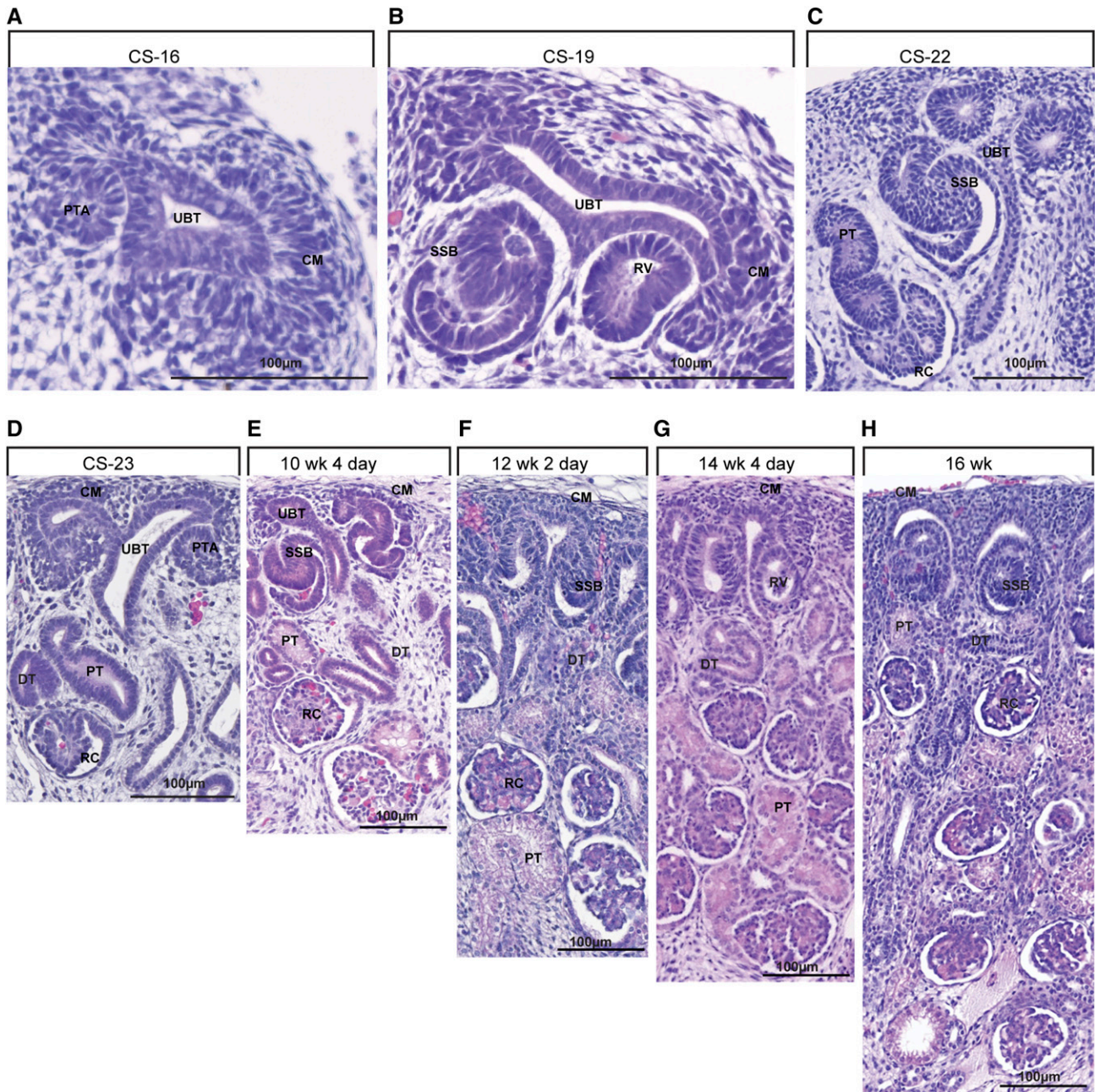


Figure 5. Histologic analyses of human kidney development show nephron formation and maturation. (A–H) Hematoxylin and eosin staining of human kidneys from CS16 to week 16 kidney as specified on fields. Magnified fields from Figure 2 have been rotated so top and bottom reflect the cortico-medullary axis. Scale bars as indicated on fields. CM, cap mesenchyme; DT, distal tubule; RC, renal corpuscle; UBT, ureteric bud tip.

nephron. With a midpoint time-frame estimate, progression from a PTA to an SSB stage would take around 8 days, with a further 5 days of development to the capillary loop stage. In contrast, in the mouse there are no nephrons at E11.5 (Supplemental Figure 1A) and clear SSB stages by E12.5 (Supplemental Figure 1B), consistent with time-lapse imaging of developing kidney^{44,45} indicating a time-span of around 24 hours from induction to SSB formation.

To better characterize the development of the first generation of nephrons, we performed whole-mount analysis of complete kidneys for JAG1 and KRT8 to visualize early nephrons (RV to SSB stages) and the ureteric epithelium, respectively, in whole kidney tile scan reconstructions from CS20 to week 11. At CS20, three branching events of the ureteric bud have generated anterior and posterior subdivisions (first branching event), and subsequent bifurcation divisions (Figure 6A).

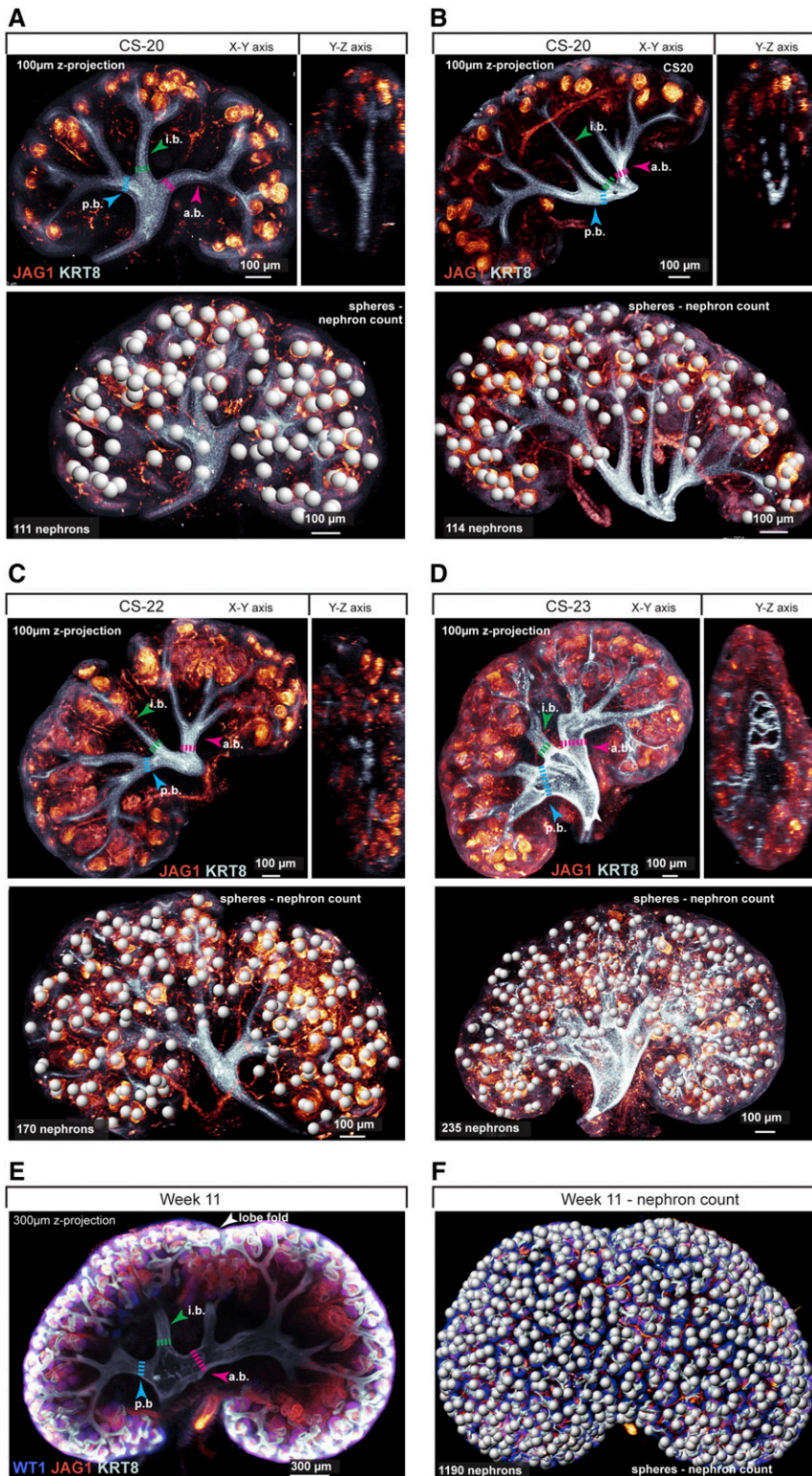


Figure 6. 3D whole-mount analyses of early human kidney development display the formation of the collecting duct system and nephrons. (A–F) Immunofluorescently labeled whole human kidneys at CS20, CS22, CS23, and week 11 stained for JAG1 to mark nascent nephrons and KRT8 to highlight the ureteric bud. The week 11 sample also stained for WT1 to mark glomeruli. Nephron counts performed using the JAG1 stains and highlighted using spheres. Nephron counts

Scoring individual JAG1+ structures indicated that the kidney contained 111 developing nephrons spanning RV to SSB stages. A second CS20 sample (Figure 6B) exhibited morphologically thinner and more elongated epithelial branch tips, although the endowment (114) and maturation of nephrons closely matched. By CS22 (Figure 6C), the ureteric bud elongated further and the kidney contained 170 nephrons ranging from RV to SSB stages.

By CS23, ureteric branch tips swelled, consistent with the histologic data discussed earlier (Figure 6D). Initiation of renal pelvis development was evident, with the early branches visible but partially engulfed within the pelvis, pointing to ongoing remodeling of the collecting duct epithelium. By week 11, an additional expansion of the pelvic region was observed (Figure 6E) and >1000 nascent nephrons could be visualized (Figure 6F); more mature nephrons evident in histologic evidence were not detected with this procedure. Video images of the whole-mount data can be viewed in the Supplemental Material.

These five samples all displayed a ureteric bud division along the anterior-posterior axis of the kidney. All specimens also displayed a single major interdomain branch projecting in a dorsal direction. Although the interdomain branch is consistently closer to the posterior domain branch point, it did not appear to project from this branch, raising the possibility that the initial division of the ureteric bud is a trifurcation in the human; trifurcations are also commonly observed in the first branching of the T-stage ureteric outgrowth in the mouse kidney^{46,47} and have been speculated to occur in humans,¹⁹ although this branch could also have emerged from the posterior domain branch, immediately after an initial bifurcation.

and scale bars as indicated on fields. a.b., anterior domain branch, indicated with dashed lines and arrowheads; i.b., interdomain branch; p.b., posterior domain branch.

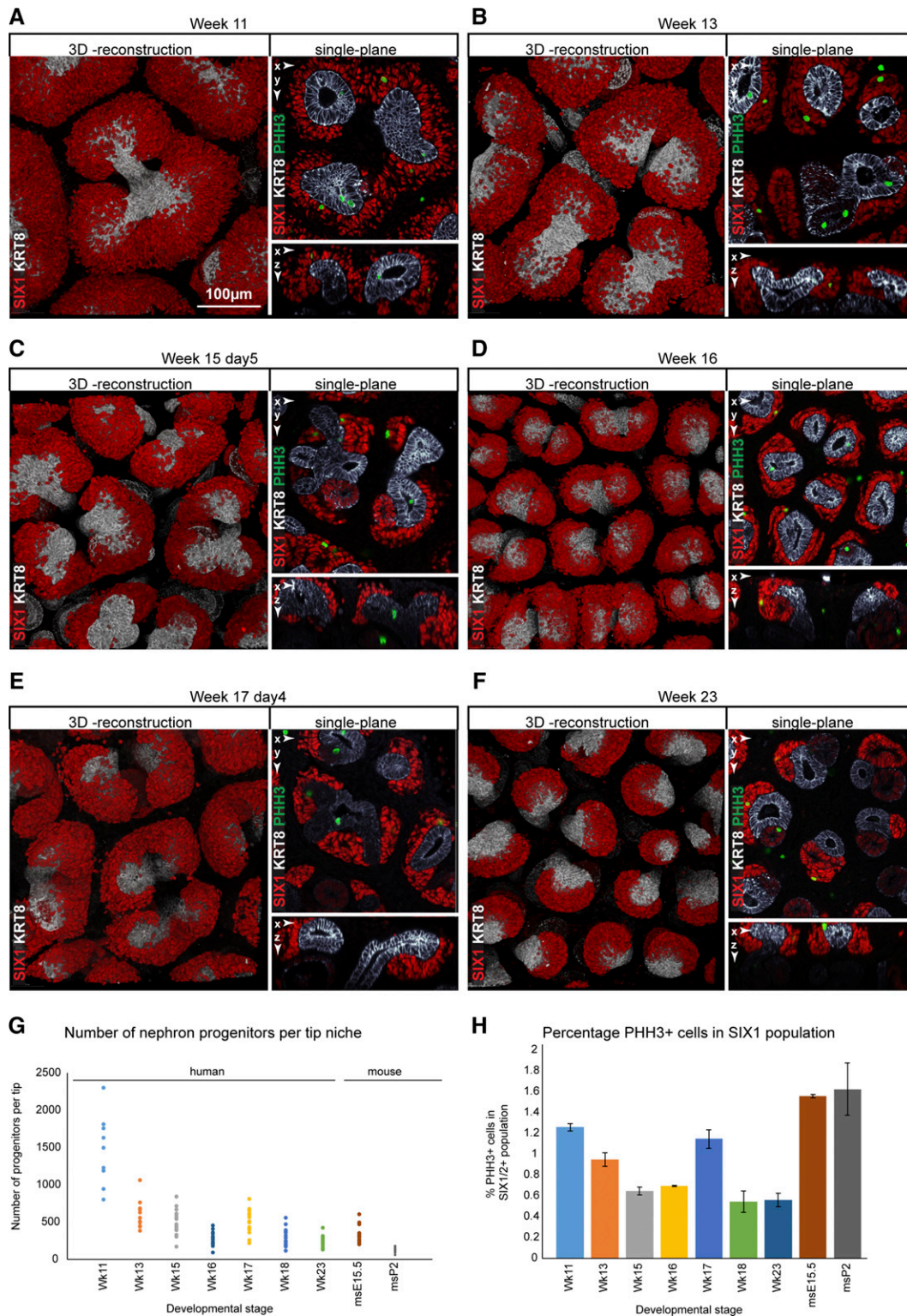


Figure 7. Three-dimensional characterization of the human nephrogenic compartment shows gradual reduction in progenitor endowment. (A–F) Whole-mount immunofluorescent stains for SIX1 and KRT8 in week 11 to week 23 kidneys. Images display a view from the top of the nephrogenic compartment looking downward toward the center of the kidney, a single confocal section, and the side-view of the niche. Single slices also display PHH3 stain. (G) Quantitative analysis of the number of nephron progenitor cells per ureteric bud tip. (H) Quantitative analysis of PHH3+ cells in the SIX1 + cell population. ms, mouse.

The Three-Dimensional Architecture of the Nephrogenic Niche

Studies in the mouse kidney have quantified cell types and cell organization in the nephrogenic niche over the period of nephrogenesis.³⁴ Over the initial period of branching, there is a reduction of nephron progenitors per ureteric epithelial branch tip, followed by a lengthy period where progenitor numbers remain approximately constant per branch tip until birth, with the cessation of branching and an accelerated commitment of progenitors to nephrogenesis. To resolve events in the human nephrogenic niche, we performed 3D confocal imaging on millimeter-thick cortical slices from kidney specimens ranging from week 11 to week 23. Slices were immunostained to visualize SIX1, a marker of nephron progenitors in the human kidney²⁸; PHH3, a marker of cells entering mitosis⁴⁸; and KRT8, highlighting the ureteric epithelial tree and distal nephron-forming structures. Human samples were compared with E15.5 and P2 mouse kidney samples to examine cross-species differences and similarities. Videos displaying the 3D architecture are included (Supplemental Material).

From week 11, the earliest stage we were able to analyze with this approach, approximately 1464 (SEM±157) SIX1⁺ nephron progenitors capped each branch tip (Figure 7, A and G). The progenitor-to-tip ratio progressively decreased to 486 (SEM±38) at week 15 (Figure 7, B, C, and G), then remained fairly constant (only a 15% drop) to week 17 (Figure 7, C–E and G). Thereafter, the progenitor tip ratio declined to 292 (SEM±27) at week 18 and 240 (SEM±14) by week 23 (Figure 7, F and G). Examining mitotic frequencies showed a decrease in the number of PHH3⁺ cells within the SIX1⁺ population over time, from approximately 1.3% at week 11 to approximately 0.5% at week 23 (Figure 7H), suggesting that decreased nephron progenitor proliferation and enhanced nephrogenesis contribute to a decrease in progenitor numbers in the nephrogenic niche. In contrast, the percentage of PHH3⁺ cells in the mouse nephrogenic niche was similar at E15.5 and P2, consistent with published studies.³⁴ Of note, the morphology and PHH3⁺ cell levels for the week 17 specimen more closely resembled a younger week 15 kidney. This observation may reflect normal sample variability in the population or some uncharacterized developmental anomaly retarding development of this kidney specimen.

The changes in nephron progenitor number/branch tip occurred alongside changes in the morphologies of both the branch tips and progenitor pool. At week 11, nephron progenitors cap large, bulbous tips (Figure 7A, Supplemental Figure 3A). As the nephron progenitor population decreased during development, progenitors tightly packed around ureteric epithelial tips, shifting to the side of the tip (Figure 7, A–F) while tips narrowed in diameter as the kidney developed. At week 23 ureteric tips pointed upwards with no sign of bifurcations. The cap-tip architecture in the week 11 human kidney most closely resembled the E15.5 mouse kidney, with a relatively large NPC population loosely positioned above the tips (Supplemental Figure 3B); whereas, the week 23 kidneys were more similar to the later P2 mouse kidney, with a small, tightly packed NPC population mainly displaced to the side of tips.

The distribution of ureteric epithelial tips across the kidney surface also changed during kidney development. Tip-to-tip distance decreased by 27% from week 11 (106 μm±SEM 1.6 μm) to week 23 (77 μm±SEM 0.7 μm) (Figure 8, A–C). Macroscopically, the distribution of tips and their nephron progenitor populations across the kidney surface displayed a rosette-like pattern of circular, radially symmetrically distributed tips; this was particularly evident at later stages, for example, at week 23. The center of the radial symmetry reflects a shared branching lineage for each cluster. Each cluster contained 2–3 tips at week 11 (Figure 8, D and E) and 5–8 tips at week 23. Interestingly, nephron progenitor cells were primarily positioned on the outward-facing surfaces of each branch tip within a cluster (Figure 8, G and H).

Human Kidney Transcriptional Profiling

To generate an overview of the gene-expression landscape during human kidney development we collected RNA from whole kidneys at five developmental stages: weeks 9, 11, 13, 17, and 21, and performed RNA-seq profiling on each sample (GEO accession numbers: GSE100859). To validate these data and determine whether genes associated with mature kidney functions could be identified, we first compared the first- and the last-stage kidneys: weeks 9 and 21. Overall gene expression was closely correlated between these samples (*R* value of 0.96; Figure 9A), although 170 genes were relatively enriched at week 9 whereas 247 genes were enriched at week 21 (Figure 9B, Supplemental Table 1; enrichment defined as two-fold higher expression at either stage). GO-term analyses highlighted cell proliferation terms in the 9-week kidneys and excretion and ion transport in the week 21 kidney, consistent with functional maturation over the 12-week developmental period (Supplemental Table 1). Multiple genes associated with nephron progenitors, interstitial progenitors, or cell proliferation were among the 170 genes enriched at week 9. Conversely, genes associated with the medullary region and nephron functionality, for example, solute carriers and transmembrane transport proteins, were identified within the 247 genes enriched at week 21.

We also performed a step-wise comparative analysis for each developmental stage against the preceding and subsequent time-point (Supplemental Tables 2 and 3). The first time-point indicating a physiologic change was week 17: a comparison of week 17 with week 13 RNA-seq generated enriched GO terms for “Excretion,” with the detection of multiple genes associated with a more mature nephron or collecting duct type; genes included: *CLCNKA*, *CLCNKB*, *UMOD*, *AQP6*, *SCNN1G*, *SCNN1B*, *ATP6V1B1*, *ATP6V0A4*, *AQP3*, *KCNJ1*, and *AQP2* (Supplemental Table 2). In summary, the broad transcriptional profiles are a rich dataset providing information that will be especially useful in assessing *in vitro* efforts to generate kidney-like structures.

Emergence of Physiologically Mature Cell Types in the Developing Human Nephron

Our data indicate that no mature nephrons are present at 8–9 weeks of development (Figure 2E); however, this is the point

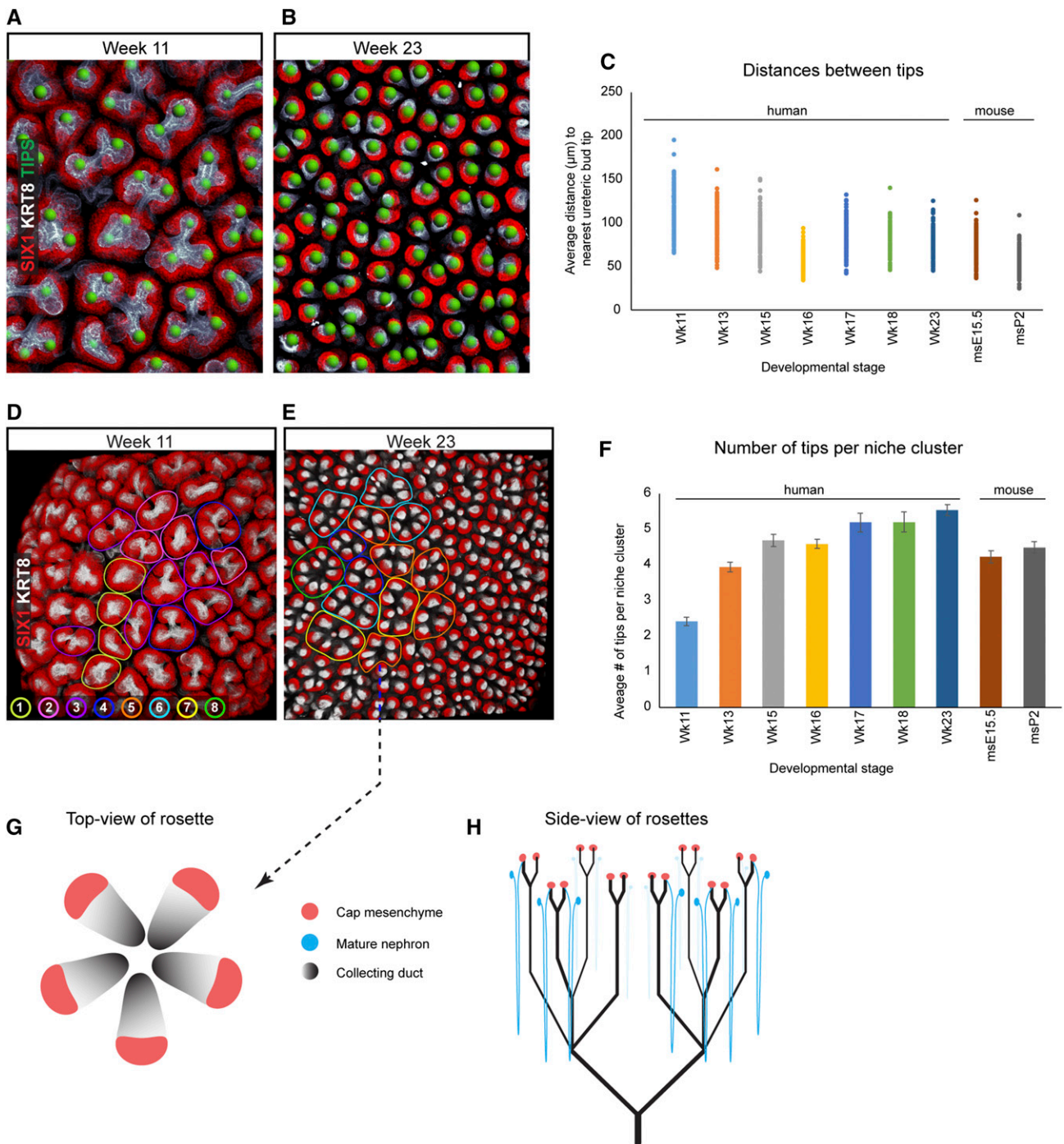


Figure 8. Three-dimensional characterization of the human nephrogenic compartment shows complex arrangements of tips and niches. Whole-mount immunofluorescent stains for SIX1 and KRT8 in week 11 to week 23 kidneys and quantitative analyses. (A, B, D, and E) Images displaying lower magnification overview of changes to the tip niche morphologies. Green spheres indicate individual terminal points of tips which were measured to analyze tip-to-nearest-tip distances. (C and F) Quantitative analysis of distances between tips and number of “tips-per-niche” during development. Colored areas in (D and E) highlight individual clusters of niches and the numbers indicate tips per cluster. (G and H) Schematic showing the top-view architecture of the rosettes and the side-view distribution of tips, niches, nascent nephrons, and mature nephrons (arcading not shown). ms, mouse.

when human kidneys have been described to become functional, as inferred from their contribution to the amniotic fluid volume.⁴⁹ To examine when cell types associated with

mature nephron identities emerge during human kidney development and to assess the degree of conservation between species, we undertook multiple approaches. First, we

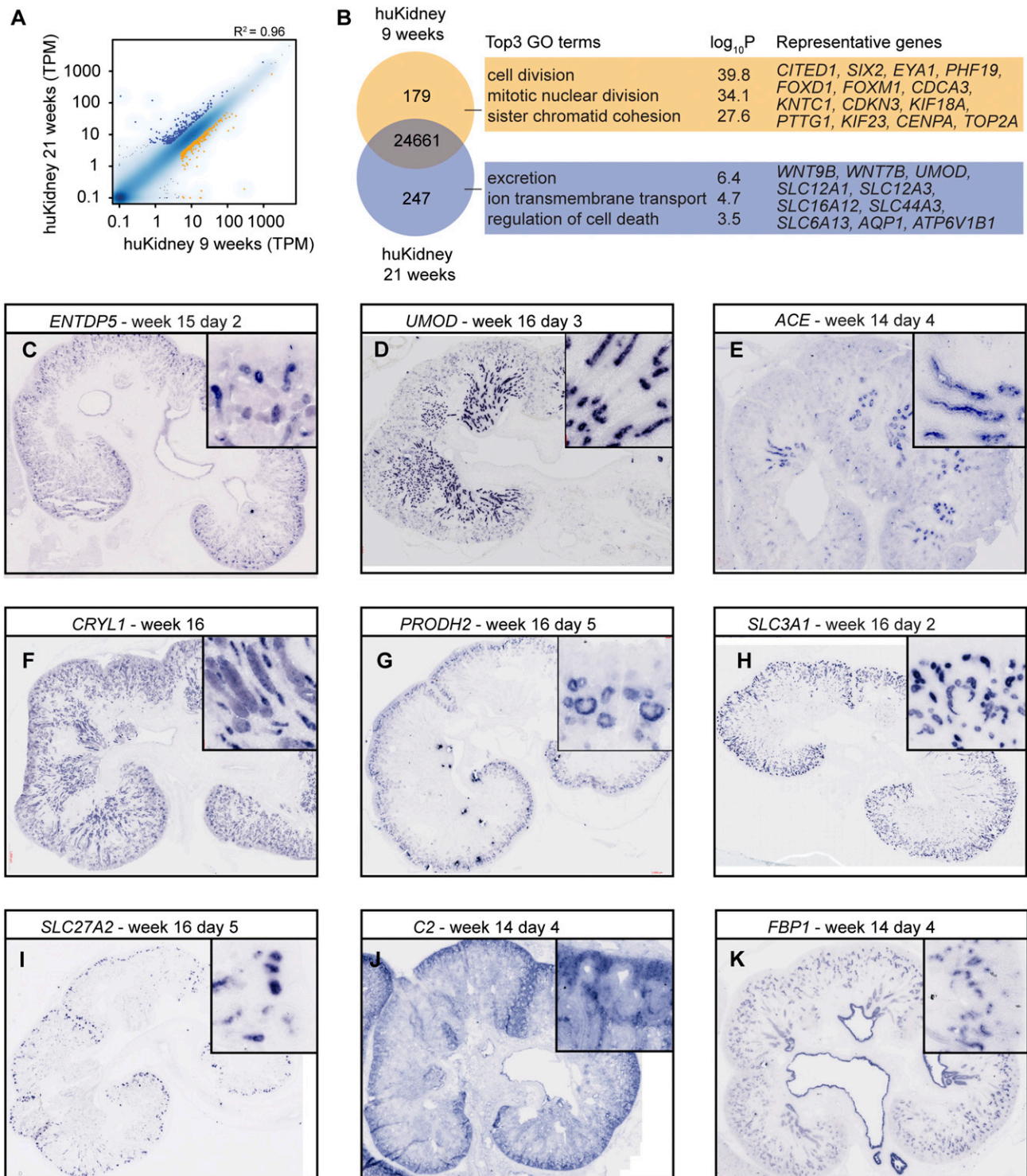


Figure 9. Identification of genes differentially expressed during maturation of human embryonic kidney. (A) Gene-level correlation of normalized mRNA-seq reads between week 9 human kidney samples and week 21 human kidney samples. (B) (Left) Number of differentially expressed genes between week 9 human kidney samples and week 21 human kidney samples. (Middle) Results of gene ontology (GO) term enrichment analysis of the indicated gene sets, with representative ones (right) from each set of genes. (C–K) Expression of genes defined as anchor genes in the mouse. Human samples range in age from week 14 day 4 to week 16 day 3. Expression and age as defined on the fields. Square inserts show magnified representative regions of nephron segments and kidney compartments that were labeled. huKidney, human kidney; TPM, Transcripts Per Kilobase Million.

performed high-resolution section *in situ* hybridizations (SISH) for 26 genes known to be expressed within the nephron lineage; so-called “anchor genes” from an earlier appraisal to identify a minimum set of nonredundant molecular markers for key cell types in the developing and adult mouse kidney.⁵⁰ Second, we analyzed the RNA from our whole-kidney RNA profiles by comparing these data to existing RNA expression profiles from specific segments of the adult rat nephron. Third, we assembled a collection of 14 antibodies that recognize epitopes of proteins that are known to be present in specific nephron segments in the mouse and performed immunofluorescent analyses on cryo-sectioned kidneys from specimens ranging from week 8 to week 16.

GUDMAP studies identified a list of 32 anchor genes on the basis of their specificity in demarcating distinct cell types in the mouse nephron and not elsewhere in the kidney.^{50,51} To determine when mature cell types emerge and whether mouse anchor genes are equivalently expressed in the human kidney, we performed SISH to visualize expression of the human counterpart of 26 of these genes; no human genes equivalent could be identified or sequence amplified for the other six (*AI317395*, *BC089597*, *Cml1*, *Ugt2b37*, *Fam129a*, and *C230096N06*). SISH was performed on >9 sections per probe on samples originating from specimens aged 9–17 weeks of development. The SISH experiments were carried out on both cryo-sectioned and wax-sectioned specimens.

Twenty of the 26 genes were detected in the human kidney (Figure 9, C–K, Table 2). Only three (11%) genes displayed a directly comparable expression between mouse and human kidneys: *SLC22A6*, *ENTPD5*, and *UMOD* (Figure 9, C and D, Table 2; and data not shown). Six genes (23%) recapitulated the mouse expression domain but displayed additional expression not documented in the mouse, whereas 11 (42%) were expressed in what is likely a different cell population and six (23%) were not detected in the human SISH kidney studies. Data highlighting distinct expression domains for *ACE*, *CRYL1*, *PRODH2*, *SLC3A1*, *SLC27A2*, *C2*, and *FBP1* are presented in (Figure 9, E–K), and data for all anchor genes are summarized in Table 2. As examples, *FBP1* and *C2* demarcate proximal tubule (PT) domains in the mouse kidney: *FBP1* was expressed in human PT, but also more broadly within the renal pelvis and renal calyces and the loop of Henle (Figure 9K), whereas *C2* was absent from the PT but expressed strongly in both nephron and interstitial progenitor compartments (Figure 9J). Genes that were not detected by SISH (*FMO2*, *MOGAT2*, *SLC18A1*, *SLC6A20*, *SPP2*, and *NPY*) showed low or undetectable transcript levels in the week 9 to week 21 whole-kidney RNA-seq data, consistent with the negative SISH result. Analysis of individual National Center for Biotechnology Information adult gene tissue summaries suggests none of these genes are strongly expressed in adult kidney (RPKM values of 5 or less).

To extend rodent and human comparisons, we compared nephron segment RNA profiles from the rat and our human

kidney RNA-seq data, analyzing expression of 56 genes highlighted in the rat nephron for distinct expression within specific rat nephron segments.⁵² Whole expression profiles are included in Supplemental Table 3. Over the week 9 to week 21 period, the proportions of different cell types change in the kidney^{19,22,23} and it is therefore challenging to directly deduce the emergence of mature cell types from whole-tissue RNA samples. However, the expectation would be that mature cell types of the various segments of the adult nephron remain rare at week 9, increasing with developmental age, with a concomitant increase in the expression of genes associated with each cell type.

We arrange the 56 genes into their respective expression domains (Supplemental Figure 4) as previously described for the rat.⁵² Genes specific to the renal corpuscle, such as *NPHS2*, *PODXL*, *MAFB*, *SYNPO*, and *NPHS1*, increased moderately and gradually over time. Genes expressed in S2–S3 segments of the PT (*PTH1R* and *HNF4A*) increased strongly from week 9 to week 11 and gradually thereafter. *SPP1* and *S100A6*, marker genes for the proximal portions of the loop of Henle, increased robustly and consistently over time. *CLU*, *UMOD*, and *SLC12A1*, expressed in the distal portion of the loop of Henle; *DEFB1*, expressed in distal convoluted tubule and connecting segment; and *AQP2*, expressed in the collecting duct, were all strongly upregulated after week 13, increasing to week 21. The data are consistent with the presence of renal corpuscles by week 11 that increase with other mature segments developing by week 11. Interestingly, many genes did not follow a coordinated behavior (e.g., *PTERG3* and *MAP3K7*) or increase over development as expected. The low level of conserved gene expression (11%), as established for the mouse anchor genes, raises the possibility that expression of several of the rat segmental marker genes may not be conserved in the developing human kidney.

To improve the resolution, we performed antibody staining on kidneys from week 8 through to week 11 and compared expression patterns against E18.5 mouse kidneys, where immature and functional nephrons are abundant. Podocytes were labeled with *MAFB* and *NPHS2* antibodies. To detect PT cells immunolabeling was performed against *LRP2* and *CUBN*,⁵³ and FITC-conjugated Lotus tetragonolobus lectin (*LTL*) was also used to label PT brush borders.⁵⁴ Distal tubules were detected using antibodies for *SLC12A1* and *SLC12A3*, whereas the ascending limb of the loop of Henle was detected using antibodies for *SLC12A1* and *UMOD*.^{55–57} The collecting duct was labeled using *KRT8*, *AQP2*, and *CALB1*; *KRT8* also demarcates the distal tubule. Vascular components within the renal corpuscle were labeled by *VEGFR2*. The distribution of these patterning markers is highlighted in Figure 10A.

AQP2+, *CALB1+*, and *KRT8+* collecting duct tubules (Figure 10, B and C) and rare *CUBN+*, *LTL+*, and *LRP2+* PTs (Figure 10, B, D, and E) were observed in the week 8 human kidney. Similarly, some morphologically immature

Table 2.

Validation of mouse anchor genes in human fetal samples.

| Gene | Ensemble Gene ID | Mouse expression | Reproduces primary expression (Yes/No) | Additional sites of expression (Yes/No) | Expression in human 14 -16 week kidney | GUDMAP Human ontology accession # |
|---------|------------------|------------------|--|---|---|-----------------------------------|
| ACE | ENSG00000159640 | EPT | No | Yes | Inner and outer medullary collecting duct; renal pelvis; proximal segment of S-shaped body | 28370, 28346, 31045, 27608, 27764 |
| ACSM1 | ENSG00000166743 | EPT | No | Yes | Inner and outer medullary collecting duct; cap mesenchyme; nephrogenic interstitium; ureteric tip | 28370, 28346, 27621, 17953, 27605 |
| BDH2 | ENSG00000164039 | EPT | Yes | Yes | Renal proximal tubule; loop of Henle; renal distal tubule | 28281, 19280, 28387 |
| CRYL1 | ENSG00000165475 | EPT | No | Yes | Inner and outer medullary collecting duct; loop of henle | 28370, 28346, 19280 |
| PRODH2 | ENSG00000250799 | EPT | No | Yes | Maturing renal corpuscle; S-shaped body | 27943, 27756 |
| SLC27A2 | ENSG00000140284 | EPT | Yes | Yes | Medial segment of S-shaped body; early proximal tubule of capillary loop nephron; loop of Henle | 27762, 315 44, 19280 |
| SLC3A1 | ENSG00000138079 | EPT | Yes | Yes | Renal proximal tubule; loop of Henle | 28281, 19280 |
| SORD | ENSG00000140263 | EPT | No | Yes | Collecting duct; renal pelvis; ureter; ureteric tip; distal segment of S-shaped body | 28407, 27608, 17950, 27605, 27760 |
| TCN2 | ENSG00000185339 | EPT | Yes | Yes | Renal proximal tubule; ureteric tip; collecting duct | 28281, 27605, 28407 |
| METTL7B | ENSG00000170439 | EPT | Yes | Yes | Renal proximal tubule; loop of Henle | 28281, 19280 |
| SLC22A6 | ENSG00000197901 | EPT | Yes | No | Renal proximal tubule (strong in S3) | 28281 |
| ENTPD5 | ENSG00000187097 | EPT | Yes | No | Medial segment of S-shaped body; renal proximal tubule | 27762, 28281 |
| C2 | ENSG00000166278 | EPT | No | Yes | Cap mesenchyme; nephrogenic interstitium; inner medullary interstitium | 27621, 17953, 28364 |
| AQP11 | ENSG00000178301 | EPT | No | Yes | Collecting duct; renal pelvis; cap mesenchyme; S-shaped body | 28407, 27608, 27621, 27756 |
| FBP1 | ENSG00000165140 | EPT | Yes | Yes | Renal pelvis; inner medullary collecting duct; renal proximal tubule | 27608, 28370, 28281 |
| FMO2 | ENSG00000094963 | EPT | No | No | Negative result - no SISH stain | n/a |
| MOGAT2 | ENSG00000166391 | EPT | No | No | Negative result - no SISH stain | n/a |
| SLC18A1 | ENSG00000036565 | EPT | No | No | Negative result - no SISH stain | n/a |
| SLC6A20 | ENSG00000163817 | EPT | No | No | Negative result - no SISH stain | n/a |
| SPP2 | ENSG00000072080 | EPT | No | No | Negative result - no SISH stain | n/a |
| GLYCTK | ENSG00000168237 | EPT | Yes | Yes | Renal proximal tubule, early proximal tubule of capillary loop nephron, loop of Henle | 28281, 31543, 19280 |
| UMOD | ENSG00000169344 | LOH | Yes | No | Loop of Henle ascending limb; renal distal tubule | 35510, 28387 |
| GPSM3 | ENSG00000213654 | RC | Yes | Yes | Renal corpuscle, inner medullary collecting duct | 27943, 28370 |
| TDRD5 | ENSG00000162782 | RC | Yes | Yes | Maturing renal corpuscle | 27943 |
| VIP | ENSG00000146469 | RC | No | Yes | Renal pelvis; collecting duct; loop of Henle | 27608, 28407, 35510 |
| NPY | ENSG00000122585 | RV | No | No | Negative result - no SISH stain | n/a |

Samples analyzed ranging in age from week 14 to week 16. Terms as previously described.⁵⁰ Ontology accession numbers for human samples as described on Gudmap.org. Green fields indicate conserved expression between mouse and human. ID, Identity; EPT, early PT; n/a, Not Applicable; LOH, Loop of Henle; RC, Renal Corpuscle.

A

| Gene | First point of detection (week 8 – week 11) | Expected mature nephron localization pattern | GUDMAP ontology # |
|----------------|---|--|-------------------|
| <i>MAFB</i> | 8 | Podocyte | 28254 |
| <i>NPFS2</i> | 8 | Podocyte | 28254 |
| <i>VEGFR2</i> | 8 | Glomerular tuft | 28239 |
| <i>LTL</i> | 8 | Renal proximal tubule | 28281 |
| <i>LRP2</i> | 8 | Renal proximal tubule | 28281 |
| <i>CUBN</i> | 8 | Renal proximal tubule | 28281 |
| <i>UMOD</i> | 10 | Loop of Henle distal straight tubule /thick ascending limb | 35512 |
| <i>SLC12A1</i> | 10 | Loop of Henle distal straight tubule /thick ascending limb | 35512 |
| <i>SLC12A3</i> | 11 | Distal convoluted tubule | 28393 |
| <i>AQP2</i> | 8 | Collecting duct | 28407 |
| <i>KRT8</i> | 8 - Detected broadly in distal nephrons | Collecting duct | 28407 |
| <i>CALB1</i> | Not detected in nephrons | Collecting duct; Renal connecting tubule | 28407; 28011 |

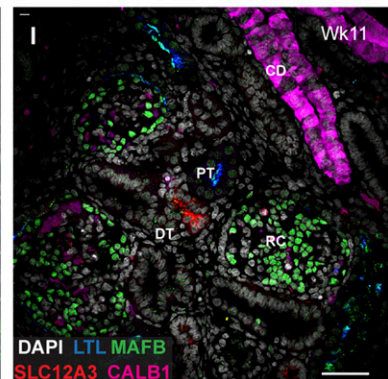
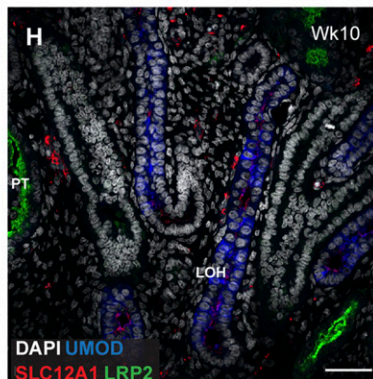
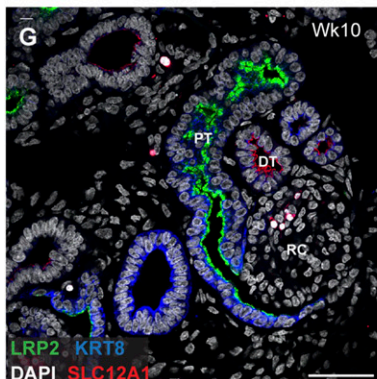
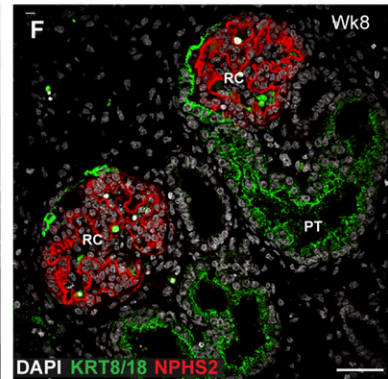
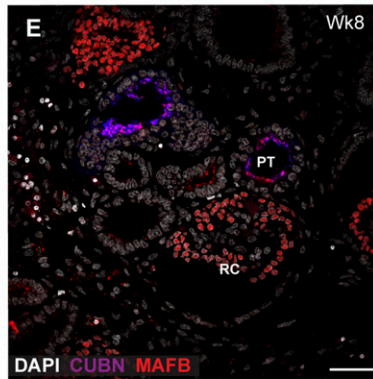
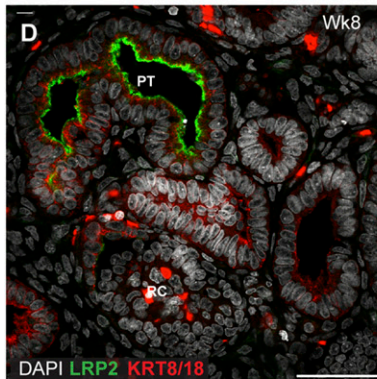
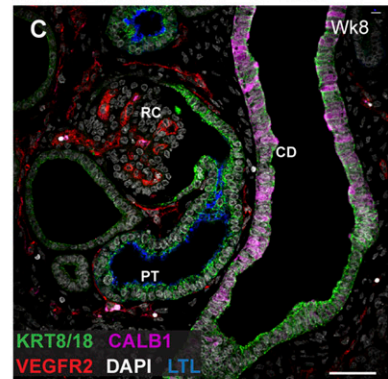
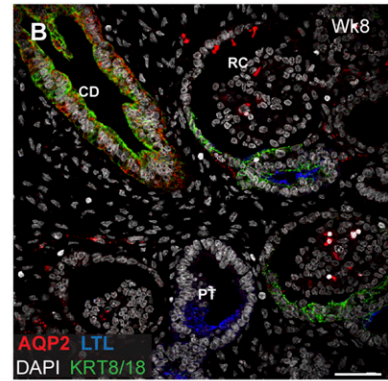


Figure 10. Kidneys from weeks 8, 10, and 11 embryos and fetuses immunostained for nephron markers indicate when mature cell types develop in the human kidney. (A) Table indicating the expected detection pattern for proteins used in figure. (B–F) Week 8. (G and H) Week 10 day 3. (I) Week 11 day 4. The antibody stains and structures are as indicated on fields. Scale bar is 50 μ m. CD, collecting duct; DT, distal tubule; LOH, loop of Henle; RC, renal corpuscle.

MAFB+, VEGFR2+, and NPHS2+ renal corpuscles were also present (Figure 10, C, E, and F). KRT8/18, specific to the mouse collecting duct, was also widely expressed in both the distal and proximal portions of nephrons (Figure 10, B–D and F). Ascending loop of Henle markers SLC12A1 and UMOD were absent until week 10 (Figure 10, G and H), and the distal tubule marker SLC12A3 until 11 (Figure 10I). Although the locations of CUBN, AQP2, and LRP2 were as expected from mouse studies, UMOD and SLC12A1 showed a reduction in their overlapping domain in the human kidney versus mouse nephron (Figure 10H, Supplemental Figure 5C). Unlike the mouse, where Calb1 is strongly detected in both the collecting duct and the connecting tubule (Supplemental Figure 5A), we did not detect human CALB1 in nephrons at these time-points.

DISCUSSION

In this study, we examined human kidney organogenesis in a large number of embryonic and fetal kidneys ranging from week 5 through to week 23, using immunohistochemistry, histology, three-dimensional modeling, and RNA profiling. Macroanatomic features are conserved in the human and mouse, albeit with distinct organization and temporal dynamics and differences in associated gene expression. We discuss these findings, contrasting human and mouse development, with a particular focus toward informing *in vitro* efforts to model human kidney development.

Nephrogenic Period *In Vivo* and in Induced NPCs

Progression to SSB nephrons takes <24 hours in the mouse kidney and in primary mouse nephron progenitor cells the process takes <48 hours when induced *in vitro*.⁵⁸ Following the progression of the first set of nephrons in the human kidney indicates nephrogenesis commences at CS16 with SSB formation at CS18–CS19, somewhat earlier than Potter²³ described. This provides an estimate of around 8 days for the transition to SSBs. The slower time course of the nephrogenic program is consistent with mouse and human comparisons in other organ systems, although the regulatory mechanisms determining the “pace of development” across mammalian species are not understood.

Comparing the Initiation of *In Vivo* and PSC-Derived *In Vitro* Nephrogenesis

Directed differentiation of nephrons has been described independently by three groups.^{11–13} Although each protocol differs in the detail, there is a common logic in WNT/FGF pathway-mediated induction of anterior or posterior intermediate mesoderm for varying times and the subsequent interaction among induced cell types to generate complex nephron-like structures over varying periods of time: 18,¹² 22,¹¹ and 16 days.¹³

In the kidney specimens analyzed, the first PTA is detected at CS16 (37–41 days postovulation), approximately 5–13 days

after the initiation of ureteric bud ingrowth into the metanephric mesenchyme. The first SSB is observed at CS18–19, or 44–51 days postovulation. The exact *in vivo* equivalent stage for human embryo-derived stem cells (ESCs) is debated, but reasonably falls between E6 postfertilization, when cells are most efficiently derived, and embryonic disc stages pregastrulation, E14, where single-cell transcriptomic analyses have placed ESCs.⁵⁹ Taking a broad and inclusive range E6–14 as a developmental starting point for ESCs and induced pluripotent cell (iPSC) equivalents,⁶⁰ if *in vitro* development reflected an *in vivo* clock, the first SSBs would appear around 30–45 days after the initiation of hIPSC/hESC differentiation. Thus, initiation of *in vitro* nephrogenesis is either relatively accelerated or *in vitro* nephron structures may be more representative of earlier formed pronephric or mesonephric kidney structures.³⁸

In the mouse, activity of Hox11 paralogs specifically demarcates the metanephric kidney anlagen and their combined action is essential for metanephric kidney development.^{61,62} Although there is strong evidence that Hox-boundaries correlate with morphologic conservation across species, the anterior extent of Hox11 expression has not been determined in the human embryo. Analysis of our RNA-seq data herein confirms the expression of HOX10/11 paralogs and absence of HOX12/13 paralogs in human kidney samples as expected from mouse studies (Supplemental Table 4). Hox11 activity in *in vitro* kidney organoids appears to vary depending on the protocol. Reanalysis of RNA-seq data from human kidney organoids profiled by Takasato *et al.*¹² shows no evidence of significant HOX11 paralog activity, although transcripts for HOX10 paralogs, and other HOX-members, are present within the dataset (see Supplemental Table 3). In contrast, immunostaining supports HOXD11 paralog activity within organoids developed by Takasato *et al.*¹² and Morizane *et al.*⁶³ *In vitro* studies will benefit from a more detailed molecular and cellular analysis of how kidney-like structures form.

A Pseudo-Stratified Ureteric Bud

We observed the appearance of a pseudo-stratified ureteric epithelium branch tip during stages CS16–CS19. Potter,²³ likewise, described a multilayered organization but concluded this to be an artifact of the high cell density and crowding of cells. However, the appearance of this structure in multiple early specimens and the disappearance at later stages suggest this is a real structural feature of the outgrowing epithelium of the human, but not the mouse, ureteric bud. Multilayered branching epithelia have been reported in the mammary gland and other branching systems.⁶⁴ After budding, the mouse ureteric bud bifurcates (or more rarely trifurcates); there then follows an extensive period of bifurcation.^{34,46} In the whole-mount analyses of human kidney specimens (CS20, week 11; Figure 6), interdomain branches do not obviously originate from either the anterior or posterior domain branches. The increased cellularity of the outgrowing human ureteric bud

might facilitate the formation of interdomain branching shortly after anterior and posterior domain branches form from the first bifurcation of the ureteric bud tip.

Mechanisms Driving Lobulation of the Human Kidney

The mechanisms driving kidney lobulation and the physiologic purpose of this process are unknown. It has been suggested that lobulation correlates with increased organism body size but exceptions to this are common.¹⁹ We detected the first sign of lobulation at CS19, when a subset of mesenchymal cells within the kidney align along the radial axis of the kidney forming striated cell clusters between the anterior and posterior domains of the kidney (arrowed in Figure 2C). The striated cells, presumably of an interstitial cell origin, pre-empt the physical separation of lobes and may therefore play a role in the formation of lobes, although addressing their function, or the triggers for their formation (local signaling and/or mechanical stresses), will be difficult to determine. After the appearance of striations, surface indentations were observed, and then actual lobes became evident anteriorly, in close proximity to the adrenal gland. Interestingly, at the level of our analysis, nephrogenic niches within interlobular or peripheral regions of the cortex were indistinguishable.

The Onset of Renal Function Corresponds with a Transitional Period of Collecting Duct Morphogenesis at CS23/Week 8

In the human kidney, we observe maturing glomeruli at an early stage of collecting duct development resembling the E12.5–E13.5 mouse kidney, 2–3 days before active functional glomeruli are present in the mouse. Previous studies have suggested human kidneys start to contribute to amniotic fluid volume at this time.⁴⁹ Further, our immunofluorescence analyses also show vascularized renal corpuscles (Figure 10) connected to PTs displaying several physiologically important proteins, *e.g.*, CUBN and LRP2. In contrast, loop of Henle marker activity, including UMOD and SLC12A1, emerged at week 10, and only at around week 11 could distal tubule marker SLC12A3 be observed (Figures 3 and 10). This suggests glomerular filtration may be occurring at CS23, but it is likely considerably later in human kidney development that the organ adopts a more mature functional activity.

Interestingly, multiple kidney specimens around CS23 and week 9 displayed characteristically expanded collecting duct morphologies distinct from other stages. This has not been described in the mouse, and is unlikely to be a prominent feature given the number of careful analyses examining mouse branching morphogenesis.³⁴ If active glomerular filtration is indeed occurring, this could lead to transient swelling of ureteric branch tips if the ureter connection to the bladder had not formed or was obstructed.^{65,66} This could also explain the observed luminal expansion which extends into stalk regions. Alternatively, altered signaling within the nephrogenic niche or interactions between tip cells and surrounding matrix could

modify branch tip morphology, and this could spread through the epithelial network.^{67,68}

The Architecture of the Developing Human Nephrogenic Niche

We observed that the 3D architecture and composition of human and mouse nephrogenic niches followed a similar developmental progression in their reduction of progenitor endowment but proceeded at different time-scales. The developmental range we described in 3D for the human occurred over approximately 80 days (11 weeks), and what we consider a comparative developmental progression occurred in the mouse within 9 days (E12.5–P2). Although we observed macroscopic similarities in the anatomy of the nephrogenic niche, absolute numbers of cellular components as well as absolute distance among anatomic structures varied across species. The number of nephron progenitors per human tip, the number of human ureteric epithelial tips, as well as distance between tips, are of a different order in the human kidney. Further, the formation of rosette-like clusters of ureteric tips (Figure 8, G and H), where nephrogenic niches face outwards, away from the center, is a distinct human feature. Given the placement of progenitors, nephron formation occurs radially around branch clusters. What accounts for this asymmetry is unclear.

Nonconserved Expression of Anchor Genes

A priority of the GUDMAP initiative has been to identify robust sets of genes to unambiguously identify discrete structures in the mouse kidney, so-called anchor genes.⁵⁰ Evaluation of human PSC- and NPC-derived kidney-like structures in kidney organoids has leaned heavily on these genes to interpret *in vitro* nephrogenesis. Surprisingly, only three of 26 anchor genes conserved what appeared to be a “mouse-like” expression pattern in the human kidney. Some prominent mouse-expressed genes like *Spp2*,⁵⁰ which encodes a secreted phosphoprotein that binds members of the Tgf- β superfamily⁶⁹ and is a specific product of a subregion of the mouse PT segment, are likely completely absent from the human kidney. This raises the question of how *Spp2* modifies kidney form, function, or physiology across species. Clearly, these differences stress the need for developing strong criteria for scoring cell diversity and identifying minimal sets of cell-type identifiers most appropriate to assess human renal kidney cell types and renal activity. This is especially important given the clinical relevance of several of these genes. For example, *SLC3A1* mutations are linked to cysteinuria⁷⁰ and *FBP1* mutations to clear cell renal cell carcinoma.⁷¹ These findings also affect interpretation of human kidney organoid development and the investment into gene reporter-driven efforts to identify and isolate critical cell types from these *in vitro* model systems. As examples, GATA3 and KRT8/18 have both been used to identify ureteric epithelial derivatives in several reports of human kidney organoids.¹² However, in contrast to the mouse, both proteins extend from the ureteric

epithelium into the distal nephron tubule, indicating that neither protein is a specific marker for the ureteric epithelial lineage (Figure 10; and data not shown).

CONCISE METHODS

Complete methods are included as Supplemental Information.

Animal Care and Embryo Collection

All animal work was reviewed and institutionally approved by Institutional Animal Care and Use Committees at the University of Southern California and performed according to institutional guidelines. Swiss Webster mice were purchased from Taconic Biosciences and maintained as a breeding colony. Timed matings were set up to recover embryos and neonates at the appropriate age.⁷²

Human Kidney Material

Consented, anonymized, human fetal tissue was obtained from elective terminations following review of the study by the Keck School of Medicine of the University of Southern California's Institutional Review Board. Kidney samples ranging in age from 4 to 23 weeks of gestation were supplied by collaborators at the Children's Hospital of Los Angeles, the University of California, San Francisco, or the Wellcome-funded Human Developmental Biology Resource center at the Institute of Genetic Medicine, Newcastle Upon Tyne, United Kingdom, and the Institute of Child Health, London, United Kingdom. Gestational age was determined per guidelines specified by the American College of Obstetricians and Gynecologists using ultrasound, heel-to-toe, and crown-to-rump measurements following published CSs.^{35–37} Stages indicate the age of the embryo or fetus from the point of conception/fertilization. Samples from the Children's Hospital of Los Angeles were received immediately after elective terminations and transported on ice at 4°C in 10% FBS, 25 mM Hepes, high-glucose DMEM (SIGMA). Samples from the University of California, San Francisco, were transported similarly by overnight courier. Samples from the Human Developmental Biology Resource center were supplied as whole tissues fixed in 4% formaldehyde and shipped in PBS, or as paraffin sections or whole tissue embedded in paraffin. Given the anonymized nature of the specimens, no further information was available regarding the specimens or the normalcy of the pregnancy.

ACKNOWLEDGMENTS

We thank all members of the McMahon lab for helpful discussions. We thank Dr. Jamie Davies (University of Edinburgh) and Dr. Qais Al-Awqati (Columbia University) for pointing out and providing copies of work by Peter, Oliver, and Reinhoff. We thank Dr. Rachel Steward and Dr. Melissa Wilson for their help providing tissue samples and Institutional Review Board approval processes. Human embryonic and fetal material was provided by the Joint Medical Research Council/Wellcome Trust (grant # 099175/Z/12/Z) Human Developmental Biology Resource (www.hdbr.org). We thank Dr. Cathy Mendelsohn (Columbia University) for histology samples.

Work in A.P.M.'s laboratory was supported by grants from the National Institutes of Health (NIH) (DK107350, DK094526, DK110792) and the California Institute for Regenerative Medicine (LA1-06536). E. R. was supported by the National Institute of Diabetes and Digestive and Kidney Diseases Award (F31DK107216). A.D.K. was supported by the NIH (5F32DK109616-02) and the University of Southern California (USC) Stem Cell postdoctoral fellowship from the Hearst Foundation. Q.G. was supported by the USC Research Enhancement Fellowship.

N.O.L., J.G., T.T., Q.G., J.A.M., and A.P.M. planned experiments and analyzed data. N.O.L., Q.G., T.T., and J.A.M. assembled the figures. N.O.L., J.A.M., J.G., R.K.P., E.R., C.L., and G.S. collected data. B.G. and L.B. provided embryonic and fetal kidneys. R.E.S. and C.K. built the image visualization tools for human data at GUDMAP.org. N.O.L. and A.P.M. wrote the manuscript, incorporating input from all authors.

DISCLOSURES

None.

REFERENCES

- Costantini F, Kopan R: Patterning a complex organ: Branching morphogenesis and nephron segmentation in kidney development. *Dev Cell* 18: 698–712, 2010
- Little MH, McMahon AP: Mammalian kidney development: Principles, progress, and projections. *Cold Spring Harb Perspect Biol* 4: 1–18, 2012
- McMahon AP: Development of the mammalian kidney. *Curr Top Dev Biol* 117: 31–64, 2016
- Kobayashi A, Valerius MT, Mugford JW, Carroll TJ, Self M, Oliver G, McMahon AP: Six2 defines and regulates a multipotent self-renewing nephron progenitor population throughout mammalian kidney development. *Cell Stem Cell* 3: 169–181, 2008
- Boyle S, Misfeldt A, Chandler KJ, Deal KK, Southard-Smith EM, Mortlock DP, Baldwin HS, de Caestecker M: Fate mapping using Cited1-CreERT2 mice demonstrates that the cap mesenchyme contains self-renewing progenitor cells and gives rise exclusively to nephronic epithelia. *Dev Biol* 313: 234–245, 2008
- Humphreys BD, Lin S-L, Kobayashi A, Hudson TE, Nowlin BT, Bonventre JV, Valerius MT, McMahon AP, Duffield JS: Fate tracing reveals the pericyte and not epithelial origin of myofibroblasts in kidney fibrosis. *Am J Pathol* 176: 85–97, 2010
- Kobayashi A, Mugford JW, Krautzberger AM, Naiman N, Liao J, McMahon AP: Identification of a multipotent self-renewing stromal progenitor population during mammalian kidney organogenesis. *Stem Cell Reports* 3: 650–662, 2014
- Sequeira Lopez ML, Cherniavsky DR, Nomasa T, Wall L, Yanagisawa M, Gomez RA: The embryo makes red blood cell progenitors in every tissue simultaneously with blood vessel morphogenesis. *Am J Physiol Regul Integr Comp Physiol* 284: R1126–R1137, 2003
- Schedl A: Renal abnormalities and their developmental origin. *Nat Rev Genet* 8: 791–802, 2007
- Bertram JF, Douglas-Denton RN, Diouf B, Hughson MD, Hoy WE: Human nephron number: Implications for health and disease. *Pediatr Nephrol* 26: 1529–1533, 2011
- Taguchi A, Kaku Y, Ohmori T, Sharmin S, Ogawa M, Sasaki H, Nishinakamura R: Redefining the in vivo origin of metanephric nephron progenitors enables generation of complex kidney structures from pluripotent stem cells. *Cell Stem Cell* 14: 53–67, 2014
- Takasato M, Er PX, Chiu HS, Maier B, Baillie GJ, Ferguson C, Parton RG, Wolvetang EJ, Roost MS, Chuva de Sousa Lopes SM, Little MH: Kidney

- organoids from human iPS cells contain multiple lineages and model human nephrogenesis. *Nature* 526: 564–568, 2015
13. Freedman BS, Brooks CR, Lam AQ, Fu H, Morizane R, Agrawal V, Saad AF, Li MK, Hughes MR, Werff RV, Peters DT, Lu J, Baccei A, Siedlecki AM, Valerius MT, Musunuru K, McNagny KM, Steinman TI, Zhou J, Lerou PH, Bonventre JV: Modelling kidney disease with CRISPR-mutant kidney organoids derived from human pluripotent epiblast spheroids. *Nat Commun* 6: 8715, 2015
 14. Sharmin S, Taguchi A, Kaku Y, Yoshimura Y, Ohmori T, Sakuma T, Mukoyama M, Yamamoto T, Kurihara H, Nishinakamura R: Human induced pluripotent stem cell-derived podocytes mature into vascularized glomeruli upon experimental transplantation. *J Am Soc Nephrol* 27: 1778–1791, 2016
 15. Osathanondh V, Potter EL: Development of human kidney as shown by microdissection. V. Development of vascular pattern of glomerulus. *Arch Pathol* 82: 403–411, 1966
 16. Osathanondh V, Potter EL: Development of human kidney as shown by microdissection. IV. Development of tubular portions of nephrons. *Arch Pathol* 82: 391–402, 1966
 17. Osathanondh V, Potter EL: Development of human kidney as shown by microdissection. III. Formation and interrelationship of collecting tubules and nephrons. *Arch Pathol* 76: 290–302, 1963
 18. Osathanondh V, Potter EL: Development of human kidney as shown by microdissection. II. Renal pelvis, calyces, and papillae. *Arch Pathol* 76: 277–289, 1963
 19. Oliver J: *Nephrons and Kidneys: A Quantitative Study of Development and Evolutionary Mammalian Renal Architectonics*, New York, Harper & Row, 1968
 20. Kampmeier OF: The metanephros or so-called permanent kidney in part provisional and vestigial. *Anat Rec* 33: 115–120, 1926
 21. Huber CG: On the development and shape of uriniferous tubules of certain of the higher mammals. *Am J Anat* 4: 1–98, 1905
 22. Peter K: *Untersuchungen über Bau und Entwicklung der Niere*, Jena, Verlag von G. Fischer, 1927
 23. Potter EL: *Normal and Abnormal Development of the Kidney*, Chicago, Year Book Medical Publishers, Inc., 1972
 24. Reinhoff WF: Development and growth of the metanephros or permanent kidney in chick embryos. *John Hopkins Hosp Bull* 381: 392–406, 1922
 25. Sperber I: Studies on the mammalian kidney, by Ivar Sperber. [Inaugural-dissertation of the philosophical faculty of the University of Uppsala.], Uppsala, Almqvist och Wiksells boktryck, 1944
 26. Schmidt-Nielsen B, O'Dell R: Structure and concentrating mechanism in the mammalian kidney. *Am J Physiol* 200: 1119–1124, 1961
 27. Beuchat CA: Structure and concentrating ability of the mammalian kidney: Correlations with habitat. *Am J Physiol* 271: R157–R179, 1996
 28. O'Brien LL, Guo Q, Lee Y, Tran T, Benazet JD, Whitney PH, Valouev A, McMahon AP: Differential regulation of mouse and human nephron progenitors by the Six family of transcriptional regulators. *Development* 143: 595–608, 2016
 29. Hughson MD, Douglas-Denton R, Bertram JF, Hoy WE: Hypertension, glomerular number, and birth weight in African Americans and white subjects in the southeastern United States. *Kidney Int* 69: 671–678, 2006
 30. Keller G, Zimmer G, Mall G, Ritz E, Amann K: Nephron number in patients with primary hypertension. *N Engl J Med* 348: 101–108, 2003
 31. Gubhaju L, Sutherland MR, Black MJ: Preterm birth and the kidney: Implications for long-term renal health. *Reprod Sci* 18: 322–333, 2011
 32. Luyckx VA, Shukha K, Brenner BM: Low nephron number and its clinical consequences. *Rambam Maimonides Med J* 2: e0061, 2011
 33. Hoy WE, Hughson MD, Bertram JF, Douglas-Denton R, Amann K: Nephron number, hypertension, renal disease, and renal failure. *J Am Soc Nephrol* 16: 2557–2564, 2005
 34. Short KM, Combes AN, Lefevre J, Ju AL, Georgas KM, Lambertson T, Cairncross O, Rumballe BA, McMahon AP, Hamilton NA, Smyth IM, Little MH: Global quantification of tissue dynamics in the developing mouse kidney. *Dev Cell* 29: 188–202, 2014
 35. O'Rahilly R, Müller F, Streeter GL: *Developmental Stages in Human Embryos: Including a Revision of Streeter's "Horizons" and a Survey of the Carnegie Collection*, Washington, DC, Carnegie Institution of Washington, 1987
 36. O'Rahilly R, Müller F: Developmental stages in human embryos: Revised and new measurements. *Cells Tissues Organs* 192: 73–84, 2010
 37. Strachan T, Lindsay S, Wilson DI: *Molecular Genetics of Early Human Development*, Oxford, BIOS Scientific Publishers, 1997
 38. Cullen-McEwen L, Sutherland MR, Black MJ: The human kidney: Parallels in structure, spatial development, and timing of nephrogenesis. In: *Kidney Development, Disease, Repair and Regeneration*, 1st Ed., edited by Little MH, San Diego, CA, Academic Press, Elsevier, 2016, pp 27–40
 39. Rumballe BA, Georgas KM, Combes AN, Ju AL, Gilbert T, Little MH: Nephron formation adopts a novel spatial topology at cessation of nephrogenesis. *Dev Biol* 360: 110–122, 2011
 40. Saxén L, Sariola H: Early organogenesis of the kidney. *Pediatr Nephrol* 1: 385–392, 1987
 41. Mugford JW, Yu J, Kobayashi A, McMahon AP: High-resolution gene expression analysis of the developing mouse kidney defines novel cellular compartments within the nephron progenitor population. *Dev Biol* 333: 312–323, 2009
 42. Chen L, Al-Awqati Q: Segmental expression of Notch and Hairy genes in nephrogenesis. *Am J Physiol Renal Physiol* 288: F939–F952, 2005
 43. Saxen L: *Organogenesis of the Kidney*, Cambridge, Cambridge University Press, 1987
 44. Lindström NO, Lawrence ML, Burn SF, Johansson JA, Bakker ER, Ridgway RA, Chang C-H, Karolak MJ, Oxburgh L, Headon DJ, Sansom OJ, Smits R, Davies JA, Hohenstein P: Integrated β -catenin, BMP, PTEN, and Notch signalling patterns the nephron. *eLife* 3: e04000, 2015
 45. Lindström NO, Carragher NO, Hohenstein P: The PI3K pathway balances self-renewal and differentiation of nephron progenitor cells through β -catenin signaling. *Stem Cell Reports* 4: 551–560, 2015
 46. Majumdar A, Vainio S, Kispert A, McMahon J, McMahon AP: Wnt11 and Ret/Gdnf pathways cooperate in regulating ureteric branching during metanephric kidney development. *Development* 130: 3175–3185, 2003
 47. Watanabe T, Costantini F: Real-time analysis of ureteric bud branching morphogenesis in vitro. *Dev Biol* 271: 98–108, 2004
 48. Gurley LR, D'Anna JA, Barham SS, Deaven LL, Tobey RA: Histone phosphorylation and chromatin structure during mitosis in Chinese hamster cells. *Eur J Biochem* 84: 1–15, 1978
 49. Brace RA, Wolf EJ: Normal amniotic fluid volume changes throughout pregnancy. *Am J Obstet Gynecol* 161: 382–388, 1989
 50. Thiagarajan RD, Georgas KM, Rumballe BA, Lesieur E, Chiu HS, Taylor D, Tang DT, Grimmond SM, Little MH: Identification of anchor genes during kidney development defines ontological relationships, molecular sub-compartments and regulatory pathways. *PLoS One* 6: e17286, 2011
 51. Brunskill EW, Aronow BJ, Georgas K, Rumballe B, Valerius MT, Aronow J, Kaimal V, Jegga AG, Yu J, Grimmond S, McMahon AP, Patterson LT, Little MH, Potter SS: Atlas of gene expression in the developing kidney at microanatomic resolution. *Dev Cell* 15: 781–791, 2008
 52. Lee JW, Chou CL, Knepper MA: Deep sequencing in microdissected renal tubules identifies nephron segment-specific transcriptomes. *J Am Soc Nephrol* 26: 2669–2677, 2015
 53. Moestrup SK, Bim H, Fischer PB, Petersen CM, Verroust PJ, Sim RB, Christensen EI, Nexø E: Megalin-mediated endocytosis of transcobalamin-vitamin-B12 complexes suggests a role of the receptor in vitamin-B12 homeostasis. *Proc Natl Acad Sci U S A* 93: 8612–8617, 1996
 54. Laitinen L, Virtanen I, Saxén L: Changes in the glycosylation pattern during embryonic development of mouse kidney as revealed with lectin conjugates. *J Histochem Cytochem* 35: 55–65, 1987
 55. Lytle C, Xu JC, Biemesderfer D, Forbush B: Distribution and diversity of Na-K-Cl cotransport proteins: A study with monoclonal antibodies. *Am J Physiol* 269: C1496–C1505, 1995

56. Pennica D, Kohr WJ, Kuang WJ, Glaister D, Aggarwal BB, Chen EY, Goeddel DV: Identification of human uromodulin as the Tamm-Horsfall urinary glycoprotein. *Science* 236: 83–88, 1987
57. Gamba G, Miyanoshita A, Lombardi M, Lytton J, Lee WS, Hediger MA, Hebert SC: Molecular cloning, primary structure, and characterization of two members of the mammalian electroneutral sodium-(potassium)-chloride cotransporter family expressed in kidney. *J Biol Chem* 269: 17713–17722, 1994
58. Davies JA, Garrod DR: Induction of early stages of kidney tubule differentiation by lithium ions. *Dev Biol* 167: 50–60, 1995
59. Nakamura T, Okamoto I, Sasaki K, Yabuta Y, Iwatani C, Tsuchiya H, Seita Y, Nakamura S, Yamamoto T, Saitou M: A developmental coordinate of pluripotency among mice, monkeys and humans. *Nature* 537: 57–62, 2016
60. Chen AE, Egli D, Niakan K, Deng J, Akutsu H, Yamaki M, Cowan C, Fitzgerald C, Zhang K, Melton DA, Eggan K: Optimal timing of inner cell mass isolation increases the efficiency of human embryonic stem cell derivation and allows generation of sibling cell lines. *Cell Stem Cell* 4: 103–106, 2009
61. Wellik DM, Hawkes PJ, Capecchi MR: Hox11 paralogous genes are essential for metanephric kidney induction. *Genes Dev* 16: 1423–1432, 2002
62. Davis AP, Witte DP, Hsieh-Li HM, Potter SS, Capecchi MR: Absence of radius and ulna in mice lacking hoxa-11 and hoxd-11. *Nature* 375: 791–795, 1995
63. Morizane R, Lam AQ, Freedman BS, Kishi S, Valerius MT, Bonventre JV: Nephron organoids derived from human pluripotent stem cells model kidney development and injury. *Nat Biotechnol* 33: 1193–1200, 2015
64. Ewald AJ, Brenot A, Duong M, Chan BS, Werb Z: Collective epithelial migration and cell rearrangements drive mammary branching morphogenesis. *Dev Cell* 14: 570–581, 2008
65. Mendelsohn C: Functional obstruction: The renal pelvis rules. *J Clin Invest* 113: 957–959, 2004
66. Chen F: Genetic and developmental basis for urinary tract obstruction. *Pediatr Nephrol* 24: 1621–1632, 2009
67. Sariola H, Saarma M: GDNF and its receptors in the regulation of the ureteric branching. *Int J Dev Biol* 43: 413–418, 1999
68. Costantini F, Shakya R: GDNF/Ret signaling and the development of the kidney. *BioEssays* 28: 117–127, 2006
69. Tian H, Li CS, Zhao KW, Wang JC, Duarte MEL, David CL, Phan K, Atti E, Brochmann EJ, Murray SS: A carboxy terminal BMP/TGF- β binding site in secreted phosphoprotein 24 kD independently affects BMP-2 activity. *J Cell Biochem* 116: 667–676, 2015
70. Bisceglia L, Purroy J, Jiménez-Vidal M, d'Adamo AP, Rousaud F, Beccia E, Penza R, Rizzoni G, Gallucci M, Palacín M, Gasparini P, Nunes V, Zelante L: Cystinuria type I: Identification of eight new mutations in SLC3A1. *Kidney Int* 59: 1250–1256, 2001
71. Li B, Qiu B, Lee DSM, Walton ZE, Ochocki JD, Mathew LK, Mancuso A, Gade TPF, Keith B, Nissim I, Simon MC: Fructose-1,6-bisphosphatase opposes renal carcinoma progression. *Nature* 513: 251–255, 2014
72. Mugford JW, Sipilä P, Kobayashi A, Behringer RR, McMahon AP: Hoxd11 specifies a program of metanephric kidney development within the intermediate mesoderm of the mouse embryo. *Dev Biol* 319: 396–405, 2008

This article contains supplemental material online at <http://jasn.asnjournals.org/lookup/suppl/doi:10.1681/ASN.2017080887/-/DCSupplemental>.